Pergamon

PII S0016-7037(02)00902-X

Kinetic and equilibrium Fe isotope fractionation between aqueous Fe(III) and hematite

Joseph L. Skulan, Brian L. Beard,* and Clark M. Johnson

Department of Geology and Geophysics, University of Wisconsin, Madison, WI 53706, USA

Abstract—Application of the Fe isotope system to studies of natural rocks and fluids requires precise knowledge of equilibrium Fe isotope fractionation factors among various aqueous Fe species and minerals. These are difficult to obtain at the low temperatures at which Fe isotope fractionation is expected to be largest and requires careful distinction between kinetic and equilibrium isotope effects. A detailed investigation of Fe isotope fractionation between $[Fe^{III}(H_2O)_6]^{3+}$ and hematite at 98°C allows the equilibrium $^{56}Fe/^{54}Fe$ fractionation to be inferred, which we estimate at $10^3 ln\alpha_{Fe(III)\text{-hematite}} = -0.10 \pm 0.20‰$. We also infer that the slope of Fe(III)-hematite fractionation is modest relative to $10^6/T^2$, which would imply that this fractionation remains close to zero at lower temperatures. These results indicate that Fe isotope compositions of hematite may closely approximate those of the fluids from which they precipitated if equilibrium isotopic fractionation is assumed, allowing inference of $\delta^{56}Fe$ values of ancient fluids from the rock record. The equilibrium Fe(III)-hematite fractionation factor determined in this study is significantly smaller than that obtained from the reduced partition function ratios calculated for $[Fe^{III}(H_2O)_6]^{3+}$ and hematite based on vibrational frequencies and Mössbauer shifts by Polyakov (1997), Polyakov and Mineev (2000), and Schauble et al. (2001), highlighting the importance of experimental calibration of Fe isotope fractionation factors. In contrast to the long-term (up to 203 d) experiments, short-term experiments indicate that kinetic isotope effects dominate during rapid precipitation of ferric oxides. Precipitation of hematite over ~12 h produces a kinetic isotope fractionation where $10^3 ln\alpha_{Fe(III)\text{-hematite}} = +1.32 \pm 0.12‰$. Precipitation under nonequilibrium conditions, however, can be recognized through stepwise dissolution in concentrated acids. As expected, our results demonstrate that dissolution by itself does not measurably fractionate Fe isotopes.   *Copyright © 2002 Elsevier Science Ltd*

1. INTRODUCTION

Several studies have documented significant mass-dependent variations in the iron isotope compositions of chemically precipitated sediments (Beard and Johnson, 1999; Zhu et al., 2000; Beard et al., in press), although the exact cause of these variations remains unclear. On the basis of Fe isotope fractionation observed during reductive dissolution of Fe minerals by the Fe-reducing bacterium *Shewenella alga* and the large variation in Fe isotope compositions of sedimentary vs. nonsedimentary rocks, Beard et al. (1999) suggested that there may be little equilibrium (abiotic) fractionation of Fe isotopes during geochemical cycling, and interpreted syn- or postdepositional biologic Fe processing as the primary cause of Fe isotope variations in rocks that formed at low temperatures. Isotopic fractionation during microbially mediated Fe mineral dissolution has been suggested by Brantley et al. (2001). However, recent investigations have also demonstrated kinetic or equilibrium Fe isotope fractionation caused by abiologic processes. These include passage of Fe solutions through ion-exchange columns (Anbar et al., 2000), formation of Fe precipitates from ferrous or ferric solutions (Skulan et al., 2000; Johnson et al., 2002; Beard et al., in press), and exchange between dissolved Fe species (Bullen et al., 2001; Johnson et al., 2002). The key to distinguishing biologic and abiologic influences on Fe isotope variations in the rock record lies in determining equilibrium and kinetic Fe isotope fractionation factors in abiotic systems, particularly between minerals and fluids.

Empirical investigations have so far been restricted to relatively simple experimental systems, involving short-term kinetic isotope effects between labile and rapidly exchanging iron pools. There are currently no empirical data on equilibrium isotope fractionation between minerals and aqueous solutions. This is a serious gap in our knowledge of the isotopic behavior of Fe, because such fractionation could strongly influence the iron isotope composition of rocks over geological time and obscure the primary Fe isotope signal in the sedimentary record. In addition, several studies (Polyakov, 1997; Polyakov and Mineev, 2000; Schauble et al., 2001) have calculated large equilibrium Fe isotope fractionations in aqueous and mineral systems on the basis of spectroscopic data.

As with the light stable isotopes of such elements as O, equilibrium Fe isotope fractionation in low-temperature fluid-mineral systems is difficult to investigate experimentally. Equilibrium fractionation is best measured in systems that can be shown to have reached full isotopic equilibrium from two directions, either in duplicate runs or through use of the "three-isotope" method (e.g., Matsuhisa et al., 1978). But full isotopic equilibrium is often not possible to attain in low-temperature fluid-mineral systems, including our Fe(III)-hematite system. Equilibrium fractionation factors can be estimated from natural minerals that formed under well-constrained conditions (e.g., Clayton and Epstein, 1961; Bao et al., 2000) or from theory (e.g., Kieffer, 1982; Polyakov, 1997; Polyakov and Mineev, 2000; Schauble et al., 2001). But in many cases, the only way to experimentally investigate low-temperature fluid-mineral equilibrium systems is through synthesis experiments under conditions that are thought to closely approach equilibrium

* Author to whom correspondence should be addressed (beardb@geology.wisc.edu).

(e.g., O'Neil, 1986; Carothers et al., 1988; Yapp, 1990). In such experiments, it is assumed that as the rate of synthesis approaches zero, kinetic isotope effects become negligible, and the observed isotopic difference between fluid and mineral approaches the equilibrium fractionation. This method has been extensively employed to calculate equilibrium fractionation factors between water and ferric (hydroxy)oxides for O and H (Yapp, 1987; Yapp, 1990; Bao and Koch, 1999) and in particular has been used to calculate equilibrium water-hematite O isotope fractionation factors from acid hydrolysis experiments that were very similar to those we have studied (Bao and Koch, 1999). The disadvantage of estimating equilibrium fractionation from synthesis experiments is the possibility that effects other than equilibrium isotopic fractionation, such as kinetic fractionation or isotopic inhomogeneity in the mineral, may contribute to the observed isotopic difference between mineral and fluid. This issue is addressed in detail below.

In this contribution, we investigate kinetic and equilibrium Fe isotope fractionation between $[Fe^{III}(H_2O)_6]^{3+}$ and Fe_2O_3 (hematite) at 98°C. The exchange of Fe between hematite and solution in our experiments is represented by the complex hydrolysis reaction:

$$2\,Fe^{3+} + 3H_2O \leftrightarrow Fe_2O_3 + 6H^+.$$
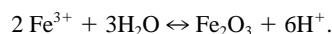
As described by Matijevic and Scheiner (1978), at temperatures above 70°C and in the absence of Cl^-, the immediate product of this reaction is hematite. We have measured Fe isotope fractionation between bulk solution and bulk hematite during both the forward reaction (pure precipitation) and backward reaction (pure dissolution). These measurements then permit us to calculate an equilibrium fractionation factor from isotopic differences observed when hematite is synthesized at slow yet varying rates via a dynamic dissolution-precipitation process.

2. METHODS

2.1. Data Representation

Iron isotope compositions for all experiments that involve isotopically "normal" Fe are expressed as $\delta^{56}Fe$ or $\delta^{57}Fe$:

$$\delta^{56}Fe = \left(\frac{^{56}Fe/^{54}Fe_{sample}}{^{56}Fe/^{54}Fe_{whole-earth}} - 1 \right) \times 1000,$$

$$\delta^{57}Fe = \left(\frac{^{57}Fe/^{54}Fe_{sample}}{^{57}Fe/^{54}Fe_{whole-earth}} - 1 \right) \times 1000.$$

The $^{56}Fe/^{54}Fe$ whole-earth ratio is the average of 46 igneous rocks ($\delta^{56}Fe = 0.0 + 0.05‰$) that range in composition from peridotite to rhyolite (Beard et al., in press).

Differences in isotope composition between Fe(III) in solution (S) and hematite (H) are expressed as $\Delta^{56}Fe$ or $\Delta^{57}Fe$:

$$\Delta^{57/56}Fe = \delta^{57/56}Fe_S - \delta^{57/56}Fe_H$$

We define $\Delta^{56}Fe^T_{S-H}$ as the "terminal $\Delta^{56}Fe_{S-H}$," that is, the value of $\Delta^{56}Fe_{S-H}$ at the end of an experimental run.

Measured isotopic differences between species can be related to isotopic fractionation factors (α) through:

$$\alpha_{S-H} = \left(\frac{1000 + \delta^{56}Fe_S}{1000 + \delta^{56}Fe_H} \right)$$

or

$$10^3 \ln\alpha_{S-H} \approx \Delta^{56}Fe_{S-H},$$

which is a good approximation over the range of isotopic compositions (several per mil) in our study. We define the instantaneous fractionation in a dynamic experiment as α^I_{S-H}, and we denote inferred kinetic fractionation as α^K_{S-H}. Inferred equilibrium fractionation is noted as α^E_{S-H}.

Several experiments used enriched ^{57}Fe tracers to measure rates of Fe exchange. These data are discussed using a modified δ notation as:

$$\delta^{57/56}Fe = \left[\frac{^{57}Fe/^{56}Fe_{sample}}{^{57}Fe/^{56}Fe_{whole-earth}} - 1 \right] \times 1000$$

and

$$\delta^{57/56}Fe_{S-H} = \delta^{57/56}Fe_S - \delta^{57/56}Fe_H.$$

2.2. Iron Isotope Analysis Methods

2.2.1. Chemical separation methods

All Fe isotope measurements were made using multiple-collector inductively coupled plasma mass spectrometry (MC-ICP-MS), with the exception of experiment 1 samples, which were made using thermal ionization mass spectrometry (TIMS). Samples must be very pure for MC-ICP-MS analysis because of potential isobars of, for example, ^{54}Cr on ^{54}Fe, $^{40}Ca^{16}O$ on ^{56}Fe, and $^{40}Ca^{16}OH$ on ^{57}Fe. To attain this purity, and especially to eliminate interferences by Cr and Ca, we modified our previously described column separation procedure (Beard and Johnson, 1999) as follows: (1) For samples smaller than 100 μg, only double-distilled or Optima-grade HCl was used. (2) After loading samples onto columns, impurities were removed by eluting in 7.0 mol/L HCl rather than 6.0 mol/L HCl. In addition, samples were collected in 10 mL of 0.5 mol/L HCl, rather than in 4 mL of 1 mol/L HCl. (3) Samples were put through chemistry twice rather than once. (4) For very small samples (<50 μg Fe), the ion-exchange chemistry was miniaturized, and a resin volume of 400 μL was used; the volume of eluants was reduced in proportion to the reduction in the volume of resin. Steps 1 to 3, which are based on procedures described by van der Walt and Strelow (1985), effectively eliminated Cr contamination, and step 4 significantly reduced blanks. We have extensively tested these ion-exchange chromatography techniques to ensure that the chemical separation method does not bias isotope compositions. Artificial samples made from ultra-pure standards that have Ca/Fe = 1 and Cr/Fe = 0.1 weight ratios with total Fe contents between 5 and 100 μg have been processed up to three times through the ion-exchange chemistry. The Fe isotope composition of these "artificial" samples is identical to the Fe isotope composition measured of the pure Fe standard that was not put through chemistry.

2.2.2. Mass spectrometry methods

Iron isotope compositions were measured using either a Mircromass Sector 54 thermal ionization mass spectrometer or a Micromass IsoProbe, a multiple-collector inductively coupled plasma mass spectrometer with a magnetic sector. Isotope analyses by TIMS used a ^{54}Fe-^{58}Fe double spike to correct for instrumental mass bias and follow the methods outlined in Beard and Johnson (1999) and Johnson and Beard (1999). External precision (1 SD) of TIMS isotope analyses is ±0.1‰/ amu (i.e., $^{56}Fe/^{54}Fe$ is ±0.2‰), as determined by replicate analysis of samples and ultrapure Fe standards (e.g., Beard and Johnson, 1999).

Iron isotope analyses measured by the IsoProbe follow the methods of Beard et al. (in press). The IsoProbe is a single-focusing multiple-collector inductively coupled plasma mass spectrometer that uses a hexapole collision cell to thermalize the ion beam so that the ion energy spread is reduced to ~1 eV. Additionally, the hexapole collision cell, with a mixture of Ar and H_2 gas, eliminates or minimizes argide ions that are isobaric with Fe (e.g., $^{40}Ar^{14}N$ at ^{54}Fe, $^{40}Ar^{16}O$ at ^{56}Fe, and $^{40}Ar^{16}OH$ at ^{57}Fe). The $^{40}Ar^{14}N$ and $^{40}Ar^{16}O$ isobars are completely eliminated by the collision cell, but a small amount of $^{40}Ar^{16}OH$ remains. The effects of the $^{40}Ar^{16}OH$ isobar are subtracted by measuring the on-peak zero of blank acid before every analysis. The magnitude of the $^{40}Ar^{16}OH$ isobar is typically 1 mV, and it varies by ±5%, and the ion intensity of the ^{57}Fe signal during an analysis is 700 mV; therefore, the variability in the on-peak zero measurement at a mass of 57 will only produce an error of ±0.004‰ for the $^{57}Fe/^{54}Fe$ ratio. Iron isotope ratios of ^{54}Fe, ^{56}Fe, and ^{57}Fe plot along mass-dependent fractionation lines, demonstrating that this on-peak zero correction technique is robust.

Iron isotope analyses were conducted on solutions diluted to a concentration of 400 ppb Fe in 0.1% HNO_3. Sample introduction is accomplished using a Cetac Aridus desolvating nebulizer fitted with an Elemental Scientific PFA spray chamber and a PFA 50 μL/min nebulizer tip (except where noted in the tables). Each analysis consists of a 1-min on-peak zero measurement using blank acid, and 30 10-s on-peak measurements using an Fe solution. The total amount of Fe consumed for an analysis is 140 ng, which includes a 1-min sample aspiration delay. Instrumental mass bias is corrected by normalizing Fe isotope ratios to the average Fe isotope composition of the standard that was run before and after the sample. The long-term external precision (1 SD) using this analysis method is $\delta^{56}Fe$ ± 0.05‰ and $\delta^{57}Fe$ ± 0.07‰, as determined by replicate analysis of samples and ultrapure standards. We routinely measure three ultrapure Fe standards; two are internal laboratory standards purchased from Johnson Mathey (UW J-M Fe) and High Purity Standards (UW HPS Fe), and the third standard is a certified isotope reference material, IRMM-014, available from the Institute for Reference Materials and Measurements (Taylor et al., 1992, 1993). Interlaboratory comparison can be made by analysis of IRMM-014. The measured Fe isotope compositions of these three standards during the course of this study were as follows: UW J-M Fe: $\delta^{56}Fe$ = 0.25 ± 0.05‰ and $\delta^{57}Fe$ = 0.39 ± 0.07‰ (1 SD, n = 47); UW HPS Fe: $\delta^{56}Fe$ = 0.49 ± 0.05‰ and $\delta^{57}Fe$ = 0.74 ± 0.07‰ (1 SD,

n = 52); and IRMM-014: $\delta^{56}Fe$ = −0.09 ± 0.05‰ and $\delta^{57}Fe$ = −0.11 ± 0.07‰ (1 SD, n = 54).

To allow direct comparison of Fe isotope composition measured for the TIMS double-spike and IsoProbe techniques, we have analyzed four samples by both methods, including a laboratory ultrapure metal standard (UW J-M Fe) and three samples (UW-Milwaukee ferrihydrite and two Pacific Fe-Mn nodules; TIMS data reported in Beard and Johnson, 1999, and Beard et al., 1999). The average difference between the IsoProbe and TIMS $\delta^{56}Fe$ values is 0.5 ± 0.2. For the purposes of this study, the bias between IsoProbe and TIMS data is not essential for our interpretations. The only Fe isotope measurements that require comparison between IsoProbe and TIMS data are the partial dissolution studies of hematite produced by rapid precipitation, and all of the TIMS data were increased by 0.5‰ for $\delta^{56}Fe$ to correct for this bias. Correction for this bias has no affect on measured Fe isotope fractionation factors.

2.3. Hematite Synthesis Experiments

2.3.1. Experimental strategy

Our experiments are fundamentally precipitation experiments in systems that approximate a steady-state condition of dissolution and precipitation. Acid hydrolysis of Fe^{3+} in dilute HNO_3 at 98°C has the advantage that hematite is the only stable mineral phase, and Fe^{3+} exists almost entirely as $[Fe^{III}(H_2O)_6]^{3+}$ because of the very weak NO_3 ligand (Hair and Beattie, 1977; Magini and Caminiti, 1977; Magini, 1978; Kanno and Hiraishi, 1982). X-ray diffraction studies have been conducted on hematite after 1 d and ~100 d of incubation. Only hematite peaks were observed, and there was no broadening of baselines that may be indicative of the presence of poorly crystalline ferrihydrite. Incubation of dilute HNO_3 and hematite was done in sealed glass containers, which were periodically harvested and immediately separated by centrifuging into hematite and solution fractions.

Because determination of isotopic fractionation factors in mineral-fluid systems at low temperatures must fundamentally rely on a synthesis approach, the eight experiments conducted were designed to evaluate Fe isotope fractionation over a range of precipitation rates and initial isotopic compositions. In general, we attempted to establish experimental conditions in which steady-state conditions of dissolution-reprecipitation were attained, and mass transfer under such conditions was calculated using ^{57}Fe-enriched materials. Average precipitation rates were varied on the basis of initial [Fe] contents in solution, the relative proportions of hematite and solution, and hematite grain size (Fig. 1, Table 1). Kinetic isotope effects during rapid precipitation were evaluated in experiment 1, which involved very rapid precipitation from solutions with high initial [Fe] (Fig. 1, Table 1). Mass transfer rates during solution-reprecipitation for average "slow" precipitation rates (Fig. 1) were established using ^{57}Fe-enriched tracers (experiment 2).

We have also attempted to constrain equilibrium Fe(III)-hematite Fe isotope fractionation through changes in initial isotope compositions of Fe(III) and hematite. For example, combining the β factors of Polyakov and Mineev (2000) and Schauble et al. (2001), a Fe(III)-hematite fractionation factor of
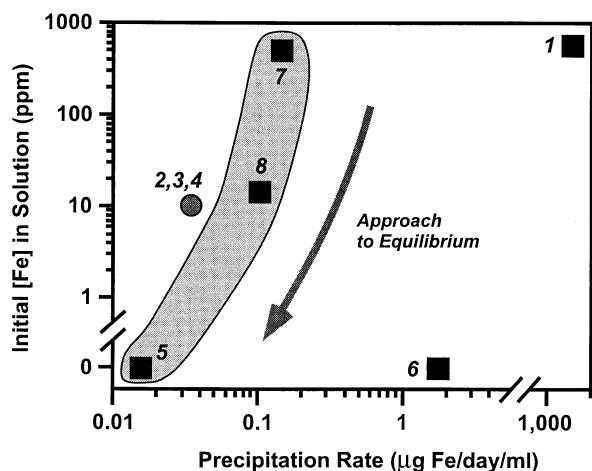
Fig. 1. Summary of initial solution [Fe] and average hematite precipitation rates for the eight experiments discussed here. Note breaks in scale; experiments 5 and 6 had no initial Fe in solution; experiment 6 used hematite with a surface area to volume ratio 13 times greater than hematite used in all the other experiments. Experiment 1 involved extremely high precipitation rates and records kinetic isotope fractionation. Experiment 2 used ^{57}Fe-enriched tracers, and experiments 3 and 4 involved starting [Fe] and hematite that had dramatically different initial isotopic compositions. On the basis of these issues, the results of experiments 5, 7, and 8 are later used to estimate the equilibrium Fe(III)-hematite Fe isotope fractionation through extrapolation to zero precipitation rates. Data given in Table 1.

+2.9‰ is predicted for ^{56}Fe/^{54}Fe at 100°C. Experiments 3 and 4 were run under conditions identical to those of experiment 2 but involved solution [Fe] that initially had very high δ^{56}Fe values of >+3.7‰ (Table 1). Two experiments involved no initial [Fe] in solution, where initial dissolution of hematite immediately produced δ^{56}Fe values of solution [Fe] that were identical to those of the starting hematite (δ^{56}Fe ~ 0‰), and these were run at low (experiment 5) and high (experiment 6) precipitation rates (Fig. 1, Table 1). Finally, in experiments 7 and 8, two different initial solution [Fe] contents were used (which produced different average precipitation rates, and the initial δ^{56}Fe values for solution [Fe] were also low (Table 1). As we will show below, the trend of Δ^{56}Fe$_{S-H}$ over time in all experiments suggests that this value is close to zero at long time periods (equilibrium). Therefore, in terms of estimation of equilibrium Fe(III)-hematite Fe isotope fractionation factors, experiments 5, 7, and 8 satisfy the requirements of low to moderate precipitation rates and small initial Fe isotope contrast (Fig. 1), which the data suggest lies closest to equilibrium conditions.

2.3.2. Experimental details

Kinetic isotope fractionation in experiment 1 used procedures that closely followed those described by Matijevic and Scheiner (1978). A solution of 10^{-2} mol/L Fe(III) in $10^{-1.3}$ mol/L HNO$_3$ was prepared from ferric nitrate salts and loaded into 10-mL Pyrex flasks that were tightly stopped, partly buried in sand that was preheated to 98°C to provide thermal mass, and placed in an oven that was preheated to 98°C. Upon heating, this solution changed from colorless to clear yellow.

Hematite precipitation began suddenly at ~3 to 5 h, the time varying between flasks. Precipitation, and the accompanying decline in solution [Fe], was initially rapid. About 80% of Fe(III) precipitated during the first hour and 95% during the first 8 h, after precipitation started. The reaction thereafter proceeded much more slowly and ceased when [Fe] had dropped to ~1% of its original value. Flasks were harvested in pairs over a period of 12 h, beginning when hematite precipitation was first noted. Hematite fractions were washed several times in double-distilled H$_2$O, and reaction progress was determined by measuring solution [Fe] using Ferrozine (Dawson and Lyle, 1990). All samples were dried, redissolved in HCl, and processed through ion-exchange chromatography (see above).

Mass transfer and Fe exchange during dissolution-reprecipitation were monitored using enriched ^{57}Fe tracers, where changes in isotope compositions were far larger than anticipated kinetic or equilibrium isotope fractionations. In experiment 2, two batches of hematite were prepared from 100 mL of starting solution using the same method used in experiment 1. To the first batch, a small amount (0.5% of total Fe) of nearly pure (93%) ^{57}Fe was added to the initial Fe(NO$_3$)$_3$-HNO$_3$ mix. An equivalent additional amount of "isotopically normal" Fe (Fe with no non-mass-dependent deviation from the isotopic composition of our whole-earth standard) was added to the second batch. ^{57}Fe-enriched and normal Fe additions were prepared from hematite or iron metal, respectively, and dissolved in 4 mol/L HCl, which was dried and redissolved in concentrated nitric acid. Each solution was placed in a Pyrex flask, sealed with a wire-secured neoprene stopper, and placed in a 98°C oven for 24 h, after which hematite and solutions were separated by centrifuging. Hematite was washed three times in double-distilled H$_2$O. The solution was centrifuged two additional times to remove residual hematite. Hematite precipitated from the ^{57}Fe-spiked solution was combined with isotopically normal solution (~10 ppm Fe) from which hematite had precipitated, in a ratio of approximately 200 μg Fe (as hematite)/mL solution, followed by vigorous shaking to keep the hematite in suspension; another suspension of isotopically normal hematite and ^{57}Fe-spiked solution was prepared in the same way. Suspensions were transferred in 5-mL aliquots to 10-mL acid-washed glass ampules, which were then heat sealed. Ampules were placed in a 98°C oven and periodically harvested over 153 d.

Experiments 3 through 8 used isotopically normal Fe. Experiment 3 was identical to experiment 2 except that no ^{57}Fe spike was used, and the hematite and solution used came from the same batch. Experiment 3 was harvested over a period of 203 d. Experiment 4 was identical to experiment 3 except that it used hematite and solution from different batches and ran for 98 d. In experiment 5, hematite was incubated with initially Fe-free solution and was prepared by mixing $10^{-1.3}$ mol/L HNO$_3$ with a small amount of concentrated HNO$_3$, which was added to increase [NO$_3$] to the level present in the initial solutions used in experiments 1 to 4. The hematite used was from the same batch as the isotopically normal hematite used in experiment 3. Experiment 5 ran for 128 d. Experiment 6 also combined hematite with an initially Fe-free solution, and the solution used was prepared as in experiment 5. However, very fine-grained, rod-shaped hematite was made by heating goe-

Table 1. Summary of acid hydrolysis experiments 1 through 8.

Experiment no.	Goal	Run time	Initial hematite (μg Fe/mL)	Initial $\delta^{56}Fe_H$	Initial [Fe] (ppm)	Initial $\delta^{56}Fe_S$	Final hematite (μg Fe/mL)	Final $\delta^{56}Fe_H$	Avg. [Fe] after first harvest (ppm)	Final $\delta^{56}Fe_S$	$\Delta^{56}Fe^T_{S\text{-}H}$	Hematite area (m²/mg)	Avg. Fe precip. rate (μg/d/mL)
1	Measure kinetic Fe isotope fractionation during rapid hematite precipitation.	12 h	0	na	563	−0.50	540	−0.40	na	3.87	4.27	0.074	na
2	[57]Fe tracer experiment, to measure the amount and average rate of Fe exchange during long-term incubation.	153 d	200	na	10	na	208	na	2.18[b]	na	na	0.074	0.035
3	Unspiked control of experiment 2.	203 d	200	−0.28	10	3.69[a]	208	0.09	2.18	2.57	2.48	0.074	0.035
4	Unspiked control of experiment 2.	98 d	200	−0.27	10	4.85	208	−0.12[c]	2.18[b]	2.71	2.83[c]	0.074	0.035
5	Long-term equilibration experiment, no initial [Fe], low Fe precipitation rate.	128 d	60	−0.28	0	na	59	−0.28	1.4	−0.07	0.21	0.074	0.016
6	Long-term equilibration experiment, no initial [Fe], high Fe precipitation rate. Used unzoned hematite.	107 d	220	−0.13	0	na	219	−0.24	0.65	0.65	0.89	0.98	1.74
7	Long-term equilibration experiment, high initial [Fe], high Fe precipitation rate.	32 d	0	na	512	0.19	511	0.34	1.3	1.20	0.86	0.074	0.150
8	Long-term equilibration experiment, moderate initial [Fe], moderate precipitation rate.	84 d	190	0.29	14.5	0.19	204	0.31	0.7	0.95	0.64	0.074	0.104

[a] The initial solution $\delta^{56}Fe$ in experiment 3 was probably higher than 3.69; the relatively low initial $\delta^{56}Fe$ measured for experiment 3 was probably caused by contamination from hematite with $\delta^{56}Fe$ close to zero; in experiment 4, which duplicates experiment 3, the initial solution $\delta^{56}Fe$ value was +4.8‰.

[b] The average [Fe] is estimated from experiment 3.

[c] $\Delta^{56}Fe^T_{S\text{-}H}$ is calculated assuming that the final $\delta^{56}Fe_H$ was −0.10‰, a value based on the measured hematite isotope composition after incubating 42 d. All Fe isotope compositions were measured using the UW Micromass IsoProbe except experiment 1. Experiment 1 isotope composition were measured using the thermal ionization mass spectrometry (TIMS) double-spike technique; TIMS double-spike values were corrected for the 0.5‰ bias between IsoProbe and TIMS values; see text for discussion.

thite for 24 h at 550°C (Ozden and Dunlop, 2000) that was prepared from KOH and $Fe(NO_3)_3 \cdot 9H_2O$ (from the same bottle used in experiments 1 to 5), following the procedure given by Schwertmann and Cornell (1991). Hematite was incubated for up to 107 d. In experiment 7, sealed 5-mL aliquots of $\sim 10^{-2}$ mol/L Fe (513.7 ppm, from Puratonic anhydrous $Fe[NO_3]_3$) in $10^{-1.3}$ mol/L HNO_3 were incubated for up to 32 d. Experiment 8 combined hematite with a solution of $10^{-1.3}$ mol/L HNO_3 and 14.5 ppm Fe (from Puratonic anhydrous $Fe[NO_3]_3$). Hematite was prepared from three ampules from experiment 7 that were harvested after 2 d of incubation, followed by leaching in 8 mol/L HNO_3 for 10 min with occasional shaking, in an attempt to remove the highly fractionated outer rim of the hematite grains that results from kinetic fractionation during the initial precipitation of hematite by acid hydrolysis (see discussion of experiment 1 below). Hematite was incubated for up to 84 d.

In all experiments, hematite settled into a thin ($<10 \ \mu m$) layer at the bottom of the incubation vessels. Vessels were not shaken during incubation, and this may have slowed the rate of iron exchange between hematite and solution. This inhibition would have affected all experiments equally and does not affect the overall interpretation of the experiments, because these interpretations depend on the relative, not the absolute, rates of exchange. Estimates of the mass of hematite in each incubation vessel were made on the basis of the masses of reagents initially used to make the hematite (Table 1). Because the mass of hematite could not be directly measured, mass estimates assume that hematite was evenly distributed in the hematite-HNO_3 suspensions from which aliquots were taken. If this assumption was not correct, masses of hematite would have varied somewhat between incubation vessels in a single experiment. Fine-grained hematite clings to most surfaces, so some hematite is lost each time a sample is transferred between containers. [Fe] measurements of solutions were made by MC-ICP-MS as part of the isotopic analysis, but because the total mass of Fe in solution samples was often 10 μg or less, Fe loss during preanalytical processing of the samples may have introduced considerable error (as high as 25%) into some of the [Fe] measurements. These errors do not, however, affect our interpretation of the experiments, where we interpret precipitation rates on the basis of hematite masses.

Scanning electron microscopy (SEM) analysis showed that the hematite produced by acid hydrolysis under our experimental conditions consisted of rounded, slightly oblong crystals with a mean diameter of approximately 225 nm (Fig. 2). These observations agree well with the results of Matijevic and Scheiner (1978). There was no significant difference in crystal size either between isotopically normal and [57]Fe-spiked hematite or between hematite that had been incubated for 150 d and hematite that had not been incubated. There was no evidence of coarsening due to Ostwald ripening. Hematite used in experiment 6, however, was prepared by heating goethite, and SEM analysis revealed that this hematite consisted of pitted, rod-shaped crystals averaging 606×73 nm (Fig. 2c) and closely resembled published photographs of hematite made by the same process (Cornell and Giovanoli, 1993). As calculated from SEM images, this hematite had a surface area of ~ 0.98 m^2/mg, ~ 13 times greater than that of hematite produced by acid hydrolysis.

Incubation did affect crystal morphology, however. The surfaces of unincubated crystals were uniformly smooth (Fig. 2a), whereas the surfaces of most of the incubated crystals were pitted (Fig. 2b). These pits ranged in shape from circular depressions with diameters of 10 to 30 nm to elongated grooves 10 to 20 nm across and up to 50 nm long. The depth of the pits could not be measured with SEM. Pits were generally arranged in a circular belt normal to the long axis of the crystals. Affected crystals typically had one to five pits, and pits appeared to be more abundant and pronounced on larger crystals. In addition to pitting, hematite from one experiment (experiment 7) appeared to have a more uneven grain size distribution after incubation, with small grains appearing as "buds" on larger ones (Fig. 2d). We interpret these smaller crystals as a second generation of crystals formed as a result of relatively rapid Fe exchange in experiment 7.

2.4. Dissolution Experiments

Isotopic inhomogeneity in natural and precipitated hematite, as well as kinetic fractionation during hematite dissolution, was investigated with acid dissolution experiments. Of particular interest was isotopic zoning within hematite crystals that was produced by rapid hematite precipitation during acid hydrolysis, which appears to follow a Rayleigh-type distillation process (experiment 1; see below).

Isotopic zoning of hematite was measured by partial dissolution in 0.9 mol/L HCl. Aliquots (0.5 mL) of this suspension were periodically removed, mixed with acetone (1 mL) to speed separation of acid and hematite, and briefly centrifuged. Full separation of acid and hematite was accomplished in < 1 min. A modified form of this experiment, in which hematite was leached in acid in 1.5-mL microcentrifuge tubes, was used to investigate possible zoning in hematite made by heating goethite (see description of experiment 6). In addition, partial dissolution using 8 mol/L HNO_3 was investigated. In all experiments, the extent of dissolution in each sample was determined on the basis [Fe] measurements by MC-ICP-MS on paired hematite and solution samples.

As a control to our partial dissolution experiments on synthesized hematite, a partial dissolution experiment was conducted on a natural specular hematite sample (origin unknown) to determine if partial dissolution by HCl produced an Fe isotope fractionation. Iron isotope homogeneity of this pebble was first established by comparing the $\delta^{56}Fe$ of several 1- to 10-mg fragments that were completely dissolved in HCl. Potential isotopic fractionation during partial dissolution was evaluated through partial HCl dissolution of a similar fragment.

3. RESULTS

We first focus on possible isotopic fractionation during partial dissolution of hematite so that we may interpret that component of the dissolution-reprecipitation process. Next, we turn to the issue of Fe isotope fractionation during very rapid precipitation. Last, we discuss the isotopic fractionations measured for the long-term incubation experiments.

3.1. Iron Isotope Fractionation During Dissolution

Dissolution of hematite in acid, by itself, is not anticipated to produce any measurable isotopic fractionation. The dissolution
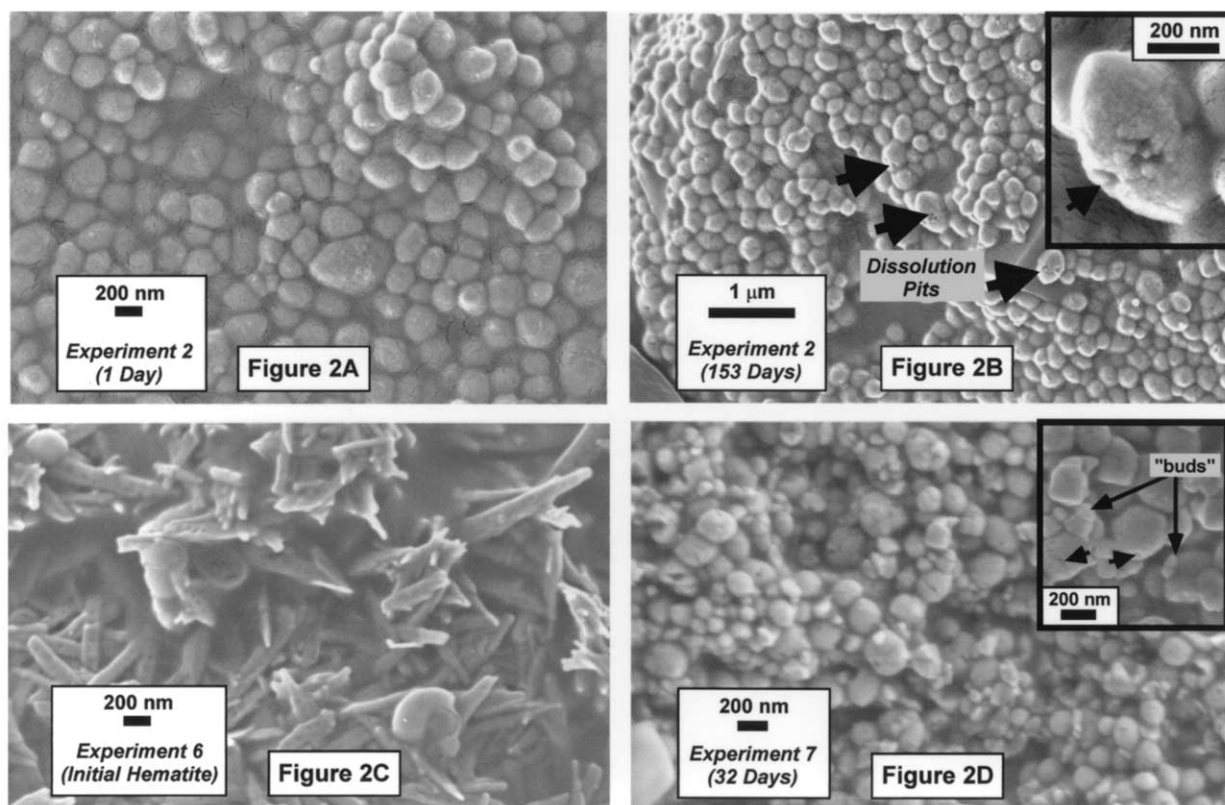
Fig. 2. Scanning electron microscopy images of hematite used in experiments. (A) Hematite grains 1 d after being formed by acid hydrolysis (experiment 2). Grains are smooth and have a relatively rounded shape and uniform size. (B) Hematite from experiment 2 after incubation in dilute HNO_3 for 153 d. The shape and size of the grains have not changed, but the surfaces of the grains are marked by numerous dissolution pits, as marked by arrows (see also inset). (C) Hematite made by dehydration of goethite, as used in experiment 6. The crystals are rod shaped, which gives them ~13 times greater relative surface area than hematite made by acid hydrolysis. These crystals also vary greatly in size. (D) Hematite grains made by acid hydrolysis and incubated for 32 d under conditions favoring a high average Fe exchange rate (experiment 7). These grains have a much greater size range than (A) or (B), which appears to reflect the growth of a second generation of crystals during incubation (see "buds" in inset). These grains also have numerous dissolution pits, as indicated by short arrows in the inset.

front advances into the mineral far faster than solid-state diffusion can occur at low temperatures, effectively preventing isotopic equilibration or adjustment between solid and dissolved Fe. If dissolution is also accompanied by precipitation, however, an isotopic contrast might be expected to develop between bulk solid and solution Fe; such a case might be applicable in near-neutral pH solutions as compared to the strong acids used here.

Complete dissolution of five fragments of a specular hematite sample yields an average $\delta^{56}Fe$ value of $-0.29 \pm 0.10‰$ (2 SD; Table 2, Fig. 3a), which suggests that this sample, at the scale of 1- to 10-mg sample sizes, is isotopically homogeneous within our estimated long-term 2-SD external reproducibility of $\pm 0.10‰$ for $\delta^{56}Fe$ values. Partial dissolution of this sample in 6 mol/L HCl at ~1 and ~10% dissolution produced $\delta^{56}Fe$ values for Fe^{3+} that are slightly lighter, averaging $-0.37‰$, although still within 2 SD of the $\delta^{56}Fe$ value for the bulk hematite. It is possible, however, that the 1- to 10-mg sample sizes used for complete dissolution masked some slight isotopic variability that was sampled by partial dissolution. Overall, we take these results to indicate that partial dissolution in concentrated HCl produces no significant isotopic fractionation, certainly $\leq 0.10‰$ (Fig. 3a).

On the basis of our results using the specular hematite sample, we can apply partial dissolution to hematite samples in our experiments, or natural samples, to investigate the extent of isotopic zonation. Partial dissolution in HCl of sample Ex 3-0 H from experiment 3 in which 98% Fe(III) precipitated within the first day, reveals significantly higher $\delta^{56}Fe$ values in the outer rim (Table 2, Fig. 3b); such high $\delta^{56}Fe$ values for the rim are consistent with the high $\delta^{56}Fe$ values ($+3.7‰$) of the remaining Fe in solution. Taking the average grain size of 200 nm after incubation for 2 d (Fig. 2), and assuming spherical geometry, the first leach step (6.8% dissolved) removed the outer 2.4 nm of the crystals. We therefore interpret the $\delta^{56}Fe$ value of $+1.2‰$ for this step to represent a very thin (<1 nm) rim that had the Fe isotope composition of the residual fluid ($+3.7‰$) and hematite that had a $\delta^{56}Fe$ value closer to zero.

Similar leaching of hematite starting material used in experiment 6 (hematite made from goethite) indicates some isotopic variability, on the order of 0.3‰ (Table 2, Fig. 3c), where one partial dissolution run (1% dissolved) produced a $\delta^{56}Fe_S$ value

Table 2. Fe isotope data for partial dissolution experiments.

Sample name	% dissolution	$\delta^{56}Fe$	$\delta^{57}Fe$	Avg. $\delta^{56}Fe$	1 SD or 2 SE
Complete dissolution of specular hematite in HCl to test for isotopic homogeneity					
Aliquot A	100	-0.28 ± 0.06	-0.41 ± 0.03	-0.28	0.06
Aliquot B	100	-0.25 ± 0.05	-0.37 ± 0.03	-0.25	0.05
Aliquot C	100	-0.23 ± 0.06	-0.34 ± 0.03	-0.24	0.01
	100	-0.25 ± 0.05	-0.31 ± 0.03		
Aliquot D	100	-0.33 ± 0.06	-0.49 ± 0.03	-0.33	0.06
Aliquot E	100	-0.35 ± 0.05	-0.47 ± 0.03	-0.34	0.02
	100	-0.33 ± 0.06	-0.48 ± 0.03		
Grand avg.				-0.29	0.05
Partial dissolution of specular hematite in HCl to test for Fe isotope fractionation					
PDSH-1 S	0.74	-0.36 ± 0.05	-0.52 ± 0.06	-0.39	0.04
	0.74	-0.41 ± 0.07	-0.58 ± 0.06		
PDSH-2 H	9.6	-0.24 ± 0.07	-0.37 ± 0.06	-0.24	0.07
PDSH-2 S	9.6	-0.31 ± 0.05	-0.57 ± 0.05	-0.36	0.05
	9.6	-0.42 ± 0.07	-0.65 ± 0.04		
	9.6	-0.39 ± 0.06	-0.46 ± 0.05		
	9.6	-0.32 ± 0.06	-0.48 ± 0.04		
Partial dissolution of hematite sample Ex 3-0 H (Table 5) made by acid hydrolysis (experiment 3) in HCl to test for isotopic homogeneity					
PDEX 1-1 H	6.8	-0.24 ± 0.06	-0.30 ± 0.04	-0.24	0.06
PDEX 1-1 S	6.8	1.16 ± 0.11	1.68 ± 0.11	1.16	0.11
PDEX 1-2 H	8.8	-0.26 ± 0.07	-0.38 ± 0.03	-0.26	0.07
PDEX 1-2 S	8.8	0.60 ± 0.08	1.02 ± 0.09	0.60	0.08
PDEX 1-3 H	19.4	-0.34 ± 0.08	-0.55 ± 0.04	-0.34	0.08
PDEX 1-3 S	19.4	0.15 ± 0.07	0.24 ± 0.09	0.15	0.07
PDEX 1-4 S	99.1	-0.30 ± 0.08	-0.39 ± 0.06	-0.30	0.08
Partial dissolution of hematite made from goethite (experiment 6) in HCl to test for isotopic homogeneity					
HFG 1-0	100	-0.12 ± 0.11	-0.11 ± 0.08	-0.13	0.03
	100	-0.15 ± 0.05	-0.25 ± 0.04		
HFG 1-1 H	1.0	-0.23 ± 0.06	-0.36 ± 0.03	-0.23	0.06
HFG 1-1 S	1.0	0.11 ± 0.03	0.15 ± 0.03	0.11	0.03
HFG 1-2 H	92	-0.33 ± 0.06	-0.47 ± 0.04	-0.33	0.06
HFG 1-2 S	92	-0.34 ± 0.05	-0.40 ± 0.03	-0.30	0.06
	92	-0.26 ± 0.05	-0.35 ± 0.03		
Partial dissolution of hematite made by acid hydrolysis (2-d incubation in experiment 7) in HNO_3 to test for isotopic homogeneity					
PDNO3 H	0.17	0.30 ± 0.08	0.49 ± 0.05	0.29	0.01
	0.17	0.28 ± 0.10	0.40 ± 0.06		
PDNO3 S	0.17	0.87 ± 0.07	1.36 ± 0.03	0.87	0.07

All data collected using the UW Micromass IsoProbe. Errors for individual analyses are 2 SE from in run statistics. Average $\delta^{56}Fe$ values are the average of two or more analyses of the same sample solution. The errors for the average $\delta^{56}Fe$ are the external (1 SD) errors; for samples that have been analyzed only once, the error is the 2 SE from the internal statistics. The sample name suffixes, H and S, refer to hematite and solution, respectively.

of $+0.11‰$, which is significantly higher than the bulk $\delta^{56}Fe$ value of $-0.13‰$; 92% partial dissolution of the same hematite produced supernatant and residual hematite that were isotopically identical (Fig. 3c). Finally, partial dissolution of hematite produced in experiment 7 was done using 8 mol/L HNO_3, and this revealed a high $\delta^{56}Fe$ outer rim (up to $+0.87‰$) that was shifted toward that of the solution after 2 d of incubation in experiment 7 (Fig. 3c). We note that partial dissolution using HNO_3 may sample different physical domains in hematite, where attack with HNO_3 concentrates on pits that penetrate the interior of the crystal (Fig. 2), whereas such pitting is absent during HCl attack (Cornell and Giovanoli, 1993), suggesting that HCl leaching may more consistently strip outer layers.

3.2. Kinetic Fe Isotope Fractionation

The results of experiment 1 (Table 3, Fig. 4) demonstrate that during rapid precipitation of hematite, $10^3 \ln\alpha^K_{S-H} =$ $+1.32 \pm 0.12‰$ under the conditions of experiment 1. We take the regressed α^K_{S-H} as an average for experiment 1 because precipitation rate was variable over the course of the experiment. We interpret the $+1.32‰$ fractionation to be a kinetic effect because the long-term incubation experiments indicate that the Fe(III)-hematite fractionation converges to smaller values over time (Fig. 5). Moreover, rapid precipitation of hematite does not allow isotopic equilibrium to be maintained between crystals and liquid, as shown by the fact that partial leaching experiments reveal strong Fe isotope zonation in rapidly precipitated hematite. Partial leaching of hematite (98% precipitation) prepared as the starting material for experiment 3 (Ex 3-0 H), which should be nearly identical to sample 6 of experiment 1 (Table 3), indicates large core-to-rim isotopic zonation (Fig. 3b). These results demonstrate that simple precipitation experiments, such as those reported for ferrihydrite precipitation over short time scales (e.g., Bullen et al., 2001), most likely reflect substantial kinetic isotope effects rather than pure equilibrium Fe isotope fractionation; kinetic isotope frac-
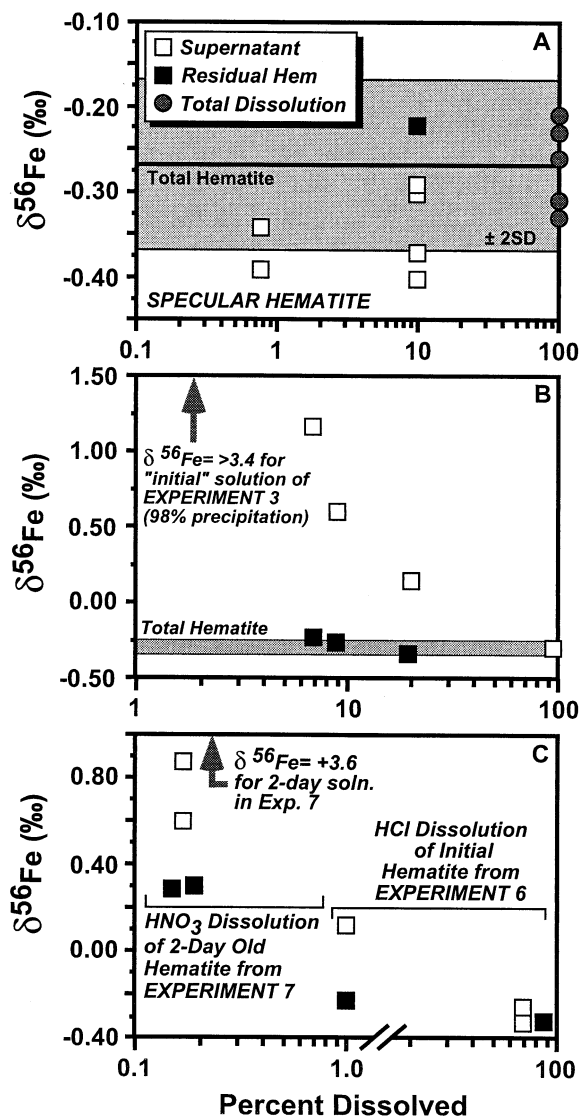
Fig. 3. Partial dissolution experiments to test for isotopic fractionation upon dissolution or isotopic zonation in minerals (Table 2). Note different scales for each figure. (A) Total dissolution of 1- to 10-mg fragments of a specular hematite sample indicates homogeneity in Fe isotope compositions within 2 SD error of our measurements. Partial dissolution in HCl indicates that isotopic heterogeneity in this sample and/or net fractionation during partial dissolution is < 0.1‰. Shaded field is the 2 SD error of our long-term reproducibility for Fe isotope analyses (±0.10‰). (B) Partial dissolution in HCl of hematite sample Ex 3-0 H (experiment 3, Table 5), which reflects 98% Fe precipitation. Sample should be very similar to sample 6 of experiment 1. The high $\delta^{56}Fe$ values in the outer rim are consistent with the high $\delta^{56}Fe$ of the solution (Ex 3-0 S), which was at least +3.4‰ (Table 1). Shaded field is the 2 SD error for long-term reproducibility (±0.10‰). (C) Partial dissolution of hematite from experiments 6 and 7 in concentrated HCl and HNO$_3$, respectively. Hematite from experiment 7 was harvested after 2 d of incubation. Data indicate that outer layers have slightly higher $\delta^{56}Fe$ values as compared to the cores. Note that data for 92% dissolution (Table 2) are offset for clarity, and note the break in scale for percentage hematite dissolved.

tionation effects may be revealed by stepwise leaching of minerals in concentrated acid. Such an approach may also determine isotopic zoning in natural minerals as a means of distinguishing kinetic vs. equilibrium Fe isotope fractionations in nature.

3.3. Estimating Equilibrium Isotope Fractionation

In all of the long-term incubation experiments, the $\Delta^{56}Fe_{S-H}$ values converge toward each other over time, regardless of the isotopic compositions of the initial starting materials (Fig. 5, Tables 5 to 10). It is particularly noteworthy that the experiment that involved the slowest precipitation rates and minimal isotopic contrast in the initial starting materials (experiment 5; Fig. 1, Tables 4–10) produced the closest convergence in $\delta^{56}Fe$ values of Fe(III) and hematite over time (Fig. 5). These observations are not consistent with the $[Fe^{III}(H_2O)_6]^{3+}$-hematite fractionation of +2.9‰ at 100°C that is predicted from the β factors of Polyakov and Mineev (2000) and Schauble et al. (2001); if this predicted fractionation were correct, then the $\Delta^{56}Fe_{S-H}$ values for experiments 5 to 8 should have increased rather than decreased with time (Fig. 5). We infer that the large $\Delta^{56}Fe_{S-H}$ values measured for experiments 3 and 4 are dominated by the "memory" of the large initial isotopic contrast, which could not be erased over the time scales of our experiments, and we do not consider these experiments further in our discussion.

A critical observation is that the final $\Delta^{56}Fe_{S-H}$ values ($\Delta^{56}Fe^T_{S-H}$) are markedly lower than that measured for kinetic fractionation (experiment 1) for those experiments in which either there was no initial Fe in solution or the isotopic composition of the solution Fe was close to that of starting hematite (experiments 5 to 8; Figs. 5c to 5f, Table 1). Because there is no fractionation during dissolution (see above), these trends could only be produced if the fractionation factor during precipitation (α^I_{S-H}) was changing with time. As explained in the next section, the most significant change that occurs during experimental runs is a drop in the hematite precipitation rate. This indicates that the fractionation factor (α^I_{S-H}) is a function of precipitation rate.

3.3.1. Mass transfer during hematite synthesis

The observation that [Fe] contents in solution quickly reach steady-state conditions from either high initial concentrations or no initial [Fe] provides support for a dissolution-reprecipitation mechanism of Fe "exchange" in the long-term experiments. The fluxes involved in such a process may be quantified using ^{57}Fe-enriched tracers because the range in $\delta^{57/56}Fe$ values is 1 to 2 orders of magnitude larger than any isotopic variation that could reasonably be attributed to kinetic or equilibrium mass fractionation. In both ^{57}Fe-spiked runs (experiments 2A and 2B), $\delta^{57/56}Fe_S$ approaches $\delta^{57/56}Fe_H$ for ~80 d, at which time approximately 70% of the initial isotopic contrast between the phases has been erased (Fig. 6, Table 4). On the basis of this, we can calculate the total mass of hematite that dissolved during experiment 2. Because [Fe] remains fairly constant as $\delta^{57/56}Fe_S$ changes, hematite dissolution must be balanced by an approximately equal rate of hematite precipitation; a near steady-state mass condition between Fe produced by dissolution of original hematite and precipitation of new hematite is dynamically maintained by a balanced dissolution-precipitation process. On the basis of this balance, an average

Table 3. Fe isotope data for experiment 1 (kinetic fractionation experiment).

Sample no.	Flask no.	$\delta^{56}Fe_S$ (‰)	$\delta^{56}Fe_H$ (‰)	$\Delta^{56}_{Fe(III)\text{-hematite}}$	Fraction Fe precipitated
1	4	-0.50 ± 0.14	-1.19 ± 0.29	0.69	0.09
2	10	-0.35 ± 0.36	-1.26 ± 0.05	0.91	0.19
3	15	0.25 ± 0.05	-1.09 ± 0.36	1.49	0.54
4	19	1.25 ± 0.12	-0.61 ± 0.83	1.61	0.74
5	18	3.07 ± 0.19	-0.68 ± 0.11	3.75	0.86
6	21	3.87 ± 0.49	-0.40 ± 0.14	4.27	0.96

All Fe isotope measurements made using the thermal ionization mass spectrometry (TIMS) double-spike method; errors are based on replicate analyses of same sample solution. All $\delta^{56}Fe$ values have been adjusted by adding 0.5‰ to allow comparison between the Fe isotope measurements made using TIMS and those made using the IsoProbe, such as partial dissolution experiment of hematite Ex 3-0 H from experiment 3 (Table 2).

hematite precipitation rate may be calculated for experiment 2 on the basis of the $\delta^{57/56}Fe$ values. However, because the $\delta^{57/56}Fe$ values cease to change after 80 d, Fe mass transfer and
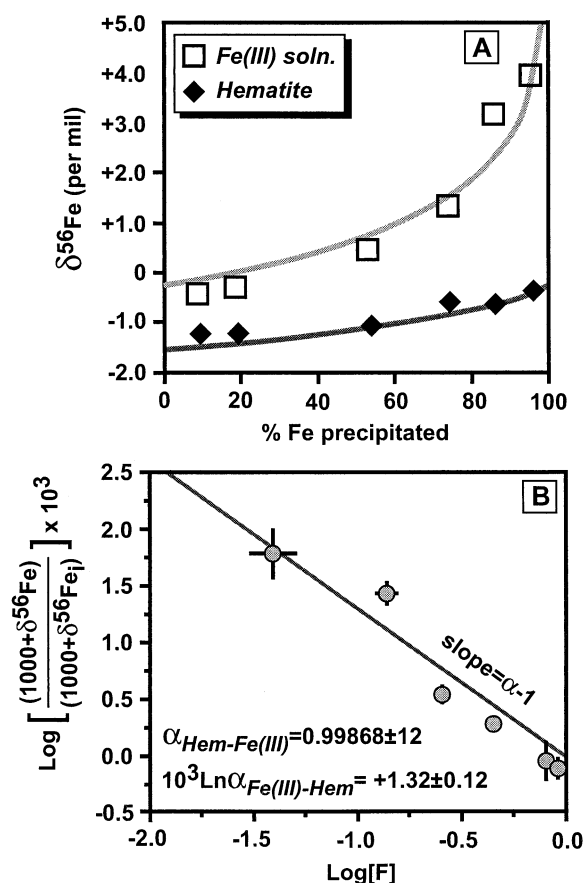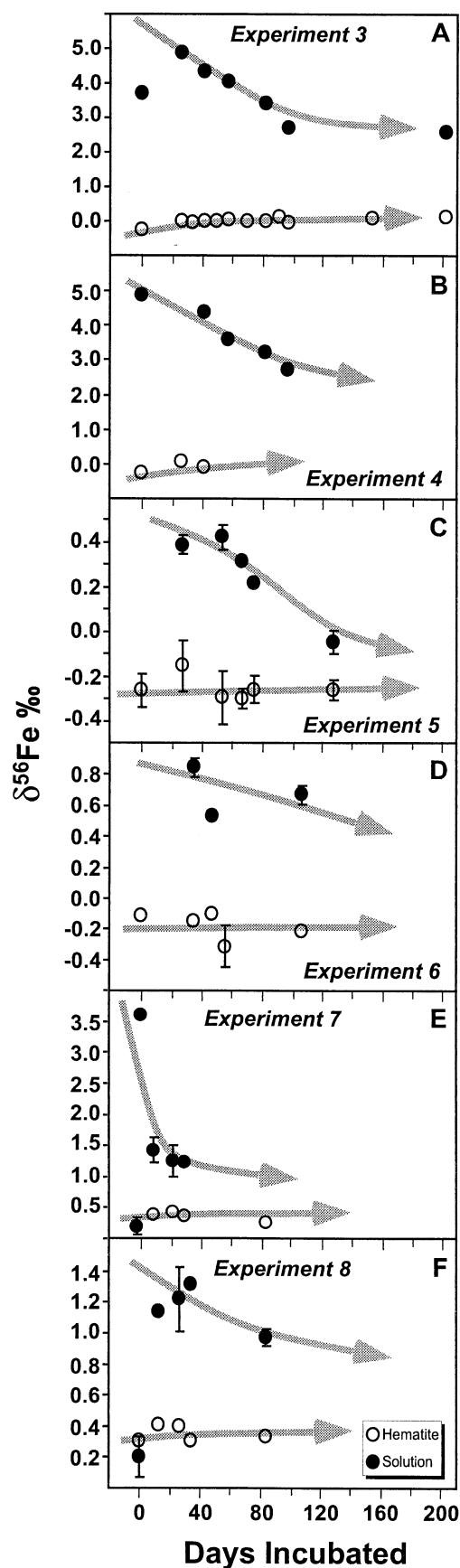

Fig. 4. Kinetic isotope fractionation experiment showing results of rapid precipitation of hematite (experiment 1; Table 3). (A) Measured $\delta^{56}Fe$ values for hematite and Fe(III) in solution. (B) Regression of data in part A, using a Rayleigh distillation equation, yields $\alpha_{HEM\text{-}Fe(III)} = 0.99868 \pm 12$, or $10^3 ln\alpha_{Fe(III)\text{-}hematite} = +1.32 \pm 0.12$‰. Error bars shown where larger than symbol. We stress that this reflects a non-equilibrium process because long-term equivalent runs (experiment 7) produce a reversal in the trend of Fe(III)-hematite fractionation over time. Moreover, the minerals produced in this experiment are isotopically zoned (see hematite sample Ex 3-0 H; Fig. 3b), which is similar to sample 6 (96% Fe precipitated) plotted here.

hence dissolution-reprecipitation processes must also cease. Therefore, the ^{57}Fe-enriched tracer experiments clearly show that the rate of dissolution and reprecipitation is not constant but drops toward zero over time.

Mass transfer of Fe between solution and hematite can occur only on the surface of the hematite grains for the temperatures of our experiments. Published literature shows that in a variety of weak acids, hematite dissolution occurs through the formation of dissolution pits along crystal defects and other high-free-energy surfaces, or "active sites," on the hematite grains (e.g., Maurice et al., 1995; Dubinina and Laakshtanov, 1997; Samson et al., 2000). The SEM images confirm the presence of dissolution pits on incubated hematite grains (Figs. 2b and 2d). Estimates of the mass of hematite dissolved from pits based on SEM images agree well with calculations based on mass balance in ^{57}Fe-spiked runs (0.8% vs. 1.1% of total hematite, respectively). It is thus reasonable to conclude that mass transfer of Fe in our experiments is initiated through formation of dissolution pits, and that Fe fluxes drop to zero when the kinetics of the system cease to favor dissolution at these sites (e.g., Maurice et al., 1995). Because dissolution is a surface phenomenon, the Fe flux through the solution (which is then precipitated as "new" hematite) will be related to the total surface area of hematite in the experiment. This allows us to use ^{57}Fe-spiked data, together with surface area measurements by SEM and [Fe] data, to calculate the net mass transfer, average precipitation rates, and residence times in solution of Fe in "isotopically normal" experiments (see Table 1).

Experiments 5, 7, and 8 use hematite that was prepared under the same acid hydrolysis conditions used to make hematite for the ^{57}Fe-spiked experiment (experiment 2), and the calculated precipitation rates lie within the range of those of experiment 2 (Fig. 1). Thus, the average rates of Fe dissolution/reprecipitation and Fe residence time in solution of these experiments can be calculated with some confidence. As noted above, we do not consider the results of experiments 3 and 4 in this discussion because of the large initial isotopic contrasts in those experiments, and we further exclude the results of experiment 6 because the very high surface area (Fig. 2c) of this hematite resulted in very high precipitation rates that may be dominated by kinetic effects (Fig. 1).

The terminal $\Delta^{56}Fe_{S\text{-}H}$, or $\Delta^{56}Fe^T_{S\text{-}H}$, for experiments 5, 7, and 8 are well correlated with the average hematite precipitation rates (Fig. 7). We interpret the relationship between $\Delta^{56}Fe^T_{S\text{-}H}$ and hematite synthesis rate, as well as the change in

$\Delta^{56}Fe_{S-H}$ in the long-term experiments, as reflecting a change in α^I_{S-H} as experimental systems move from a largely kinetic to a predominately equilibrium fractionation regime. The lowest $\Delta^{56}Fe^T_{S-H}$ observed in any of our experiments (+0.21‰ in experiment 5; Figs. 5c and 7) places an upper limit on the value of α^{EQ}_{S-H}. Below, we model the dynamics of our systems to make a more precise estimate of α^{EQ}_{S-H} and also to address several potentially complicating issues.

3.3.2. Isotopic zoning of hematite crystals

Because $\Delta^{56}Fe_{S-H}$ is measured as the difference in $\delta^{56}Fe$ of the solution and the bulk hematite, and only a few percent of the hematite grain actually participates in Fe exchange, it is possible that the isotopic composition of this small fraction may significantly differ from that of the bulk grain. Our partial dissolution experiments show that all the hematite used in the long-term experiments is isotopically inhomogeneous to some degree (Fig. 3). Despite this complexity, it is unlikely that isotopic zoning had a significant effect on $\Delta^{56}Fe_{S-H}$ during the long-term experiments unless isotopic zonation was extreme. In contrast to hematite dissolution in HCl, the dissolution pits that are associated with HNO_3 seem likely to significantly reduce the effect of zoning by cutting through the heavily fractionated outer surface of a grain, thereby exposing an isotopically average hematite surface to further dissolution. Of course, any dissolution must start on the outer surface of a grain, so the first Fe dissolved from a zoned grain must have higher $\delta^{56}Fe$ values than the whole grain average. But because the long-term synthesis experiments used much weaker HNO_3 than that used in our 8 mol/L HNO_3 partial dissolution experiments and involved fractional dissolution ~5 times greater, any zoning effect in these experiments should be much smaller than that observed during partial dissolution in concentrated acid (Fig. 3c).

Comparison of experiments 5 and 6 (Figs. 5c and 5d) provides additional evidence for the lack of a zoning effect in the long-term experiments. Experiment 5 used hematite that should have been isotopically zoned, because it was prepared in the same manner as experiment 1. In contrast, experiment 6, which was intended to minimize the effect of zoning, used hematite prepared by heating goethite, which partial HCl dissolution revealed to be minimally zoned (Fig. 3c). Because both experiments started with Fe-free solution, if the effect of zoning were strong, $\Delta^{56}Fe_{S-H}$ of experiment 5 should have been signifi-

Fig. 5. Plot of measured Fe isotope compositions of hematite and solution vs. days of incubation in long-term incubation experiments 3 to 8. The details of the different experimental conditions are summarized in Table 1, and initial conditions and precipitation rates are illustrated in Fig. 1. The low $\delta^{56}Fe$ value measured for the starting solution composition in experiment 3 probably reflects hematite contamination during the separation of the supernate; experiment 4 was run under the same conditions as experiment 3. Experiments 3 and 4 involved initial solution [Fe] and hematite that had dramatically different initial isotope compositions. Experiment 6 used hematite made from goethite; this hematite has a surface area to volume ratio that is a factor of 13 greater than the hematite used in experiments 3 to 5 and 7 and 8, which produced the highest precipitation rates measured in the long-term experiments (Fig. 1). Experiment 5 involved the lowest precipitation rate (Fig. 1), and these results are interpreted to lie closest to the equilibrium Fe(III)-hematite fractionation.
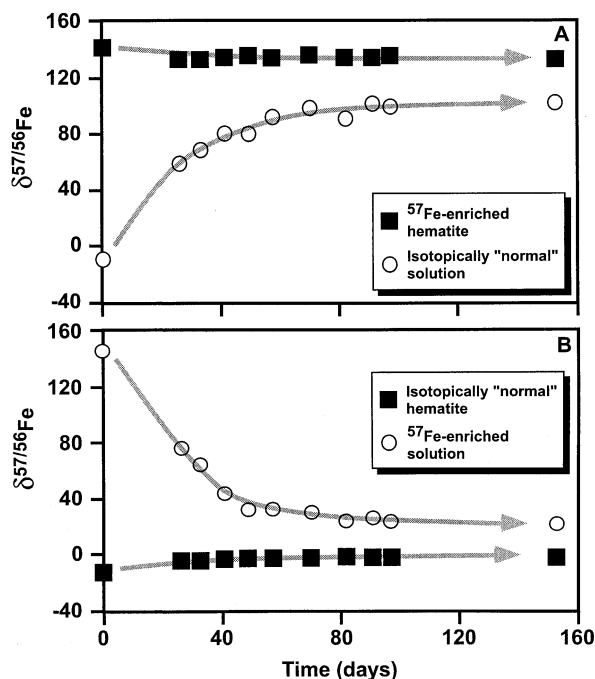
Fig. 6. Results from long-term incubation experiments using enriched ^{57}Fe as a tracer for Fe fluxes from dissolution/reprecipitation during acid hydrolysis in our experiments (experiment 2; Table 4). Because the range in isotopic compositions in the isotope tracer runs far exceeds any potential equilibrium or kinetic isotope fractionation, Fe fluxes can be well constrained using enriched tracers. Most of the Fe lies in the hematite, and therefore, the $\delta^{57/56}$Fe values shift most strongly in the solution. (A) Tracer experiment using ^{57}Fe-enriched hematite, and "isotopically normal" Fe(III). (B) Identical experiment as in part A, except that solution Fe(III) is enriched in ^{57}Fe, and initial hematite had "normal" isotope compositions.

cantly larger than that of experiment 6, but the opposite was the case. At 28 d, Δ^{56}Fe$_{S-H}$ in experiment 5 (zoned hematite) was $+0.54 \pm 0.12$‰, whereas at 35 d in experiment 6 (hematite synthesized from goethite), the Δ^{56}Fe$_{S-H}$ was $+1.00 \pm 0.08$‰.

3.3.3. Modeling changes in Δ^{56}Fe$_{S-H}$ with time

The decrease in Δ^{56}Fe$_{S-H}$ with time in all experiments is best explained by a dynamic system in which dissolution and precipitation are occurring simultaneously, but α^I_{S-H} approaches unity as the precipitation rate also decreases with time. We can simulate such a system with a flux model for Fe during incubation (Appendix, Fig. A1). The inputs for the model are estimates of Fe mass transfer rates (based on the ^{57}Fe-enriched experiments), calculated surface areas and [Fe] of the different experiments, and α^K_{S-H}, which is used as the initial value of α^I_{S-H}. The model uses iteration to predict changes in Δ^{56}Fe$_{S-H}$ as a function of Fe exchange rates and assumes that α^I_{S-H} exponentially approaches unity with time. An iterative approach simulates a time delay in the response to changing conditions, which is appropriate for acid hydrolysis under our experimental conditions. Although dissolution and precipitation rates are coupled by the effect each has on [Fe], the hydrolysis reaction requires time to initiate (see description of experiment 1), and therefore precipitation rates cannot instantaneously adjust to changes in [Fe] brought about by changes in dissolution rate, and vice versa. It is important to note that the model itself contains no assumptions about the cause of isotope fractionation but that it is based on the evidence from the

Table 4. Fe isotope data for ^{57}Fe tracer experiment (experiment 2).

Days	$\delta^{57/56}$Fe solution	$\delta^{57/56}$Fe hematite
Experiment 2A hematite made with enriched ^{57}Fe		
0	−9.2	142.2
26	59.1	133.2
33	68.8	133.1
41	80.3	134.7
49	79.7	135.8
57	92.3	134.8
70	98.4	135.3
82	90.9	134.9
91	101.6	134.2
97	99.7	135.1
153	102.3	133.4
Experiment 2B hematite made with isotopically normal Fe		
0	145.5	−12.2
26	75.8	−3.3
33	64.3	−4.1
41	44.3	−2.8
49	32.8	−2.9
57	32.4	−2.7
70	30.3	−2.8
82	24.1	−2.1
91	25.6	−1.5
97	23.5	−1.6
153	21.6	−2.2

All Fe isotope measurements were made using the UW IsoProbe with a cyclonic spray chamber and 100 μL/min PFA nebulizer tip. The precision of these isotope measurements is estimated to be ± 1‰ based on replicate analyses of solutions. The decrease in precision reflects an order of magnitude decrease in sensitivity as compared to analyses made using the Aridus desolvating nebulizer.

Table 5. Fe isotope data for long-term exchange between $[Fe^{III}(H_2O)_6]^{3+}$ and hematite (experiment 3).

Sample name	Days incubated	$\delta^{56}Fe$	$\delta^{57}Fe$	Avg. $\delta^{56}Fe$	1 SD or 2 SE
Ex 3-0 H	0	-0.33 ± 0.06	-0.55 ± 0.04	-0.28	0.07
	0	-0.23 ± 0.05	-0.38 ± 0.04		
Ex 3-0 S	0	3.71 ± 0.05	5.53 ± 0.04	3.69	0.04
	0	3.66 ± 0.10	5.41 ± 0.07		
Ex 3-1 H	27	0.01 ± 0.04	0.10 ± 0.03	-0.03	0.06
	27	-0.07 ± 0.06	-0.05 ± 0.04		
Ex 3-1 S	27	4.82 ± 0.05	7.25 ± 0.03	4.87	0.04
	27	4.87 ± 0.05	7.34 ± 0.05		
	27	4.91 ± 0.07	7.37 ± 0.04		
Ex 3-2 H	34	-0.09 ± 0.04	0.01 ± 0.03	-0.08	0.02
	34	-0.07 ± 0.08	0.02 ± 0.05		
Ex 3-3 H	42	-0.06 ± 0.05	0.00 ± 0.04	-0.04	0.04
	42	-0.01 ± 0.06	0.04 ± 0.03		
Ex 3-3 S	42	4.31 ± 0.05	6.44 ± 0.05	4.32	0.02
	42	4.34 ± 0.08	6.48 ± 0.06		
Ex 3-4 H	50	-0.04 ± 0.08	0.05 ± 0.05	-0.04	0.08
Ex 3-5 H	58	-0.02 ± 0.07	0.09 ± 0.05	0.04	0.05
	58	0.08 ± 0.07	0.10 ± 0.05		
	58	0.06 ± 0.08	0.04 ± 0.04		
Ex 3-5 S	58	3.99 ± 0.04	5.99 ± 0.04	4.03	0.04
	58	4.03 ± 0.08	6.04 ± 0.07		
	58	4.06 ± 0.07	6.09 ± 0.08		
Ex 3-6 H	71	-0.01 ± 0.07	0.04 ± 0.09	-0.04	0.04
	71	-0.07 ± 0.06	0.00 ± 0.04		
Ex 3-7 H	83	-0.06 ± 0.08	0.06 ± 0.09	-0.03	0.04
	83	0.00 ± 0.09	0.05 ± 0.05		
Ex 3-7 S	83	3.41 ± 0.05	5.16 ± 0.05	3.41	0.05
Ex 3-8 H	92	0.10 ± 0.11	0.21 ± 0.06	0.10	0.11
Ex 3-9 H	98	-0.12 ± 0.11	-0.01 ± 0.11	-0.06	0.08
	98	-0.01 ± 0.08	0.12 ± 0.04		
Ex 3-9 S	98	2.63 ± 0.05	4.07 ± 0.05	2.67	0.05
	98	2.71 ± 0.11	4.16 ± 0.08		
Ex 3-10 H	154	0.08 ± 0.08	0.15 ± 0.04	0.08	0.08
Ex 3-11 H	203	0.09 ± 0.14	0.01 ± 0.10	0.09	0.14
Ex 3-11 S	203	2.57 ± 0.06	3.84 ± 0.05	2.57	0.03
	203	2.60 ± 0.05	3.93 ± 0.04		
	203	2.54 ± 0.06	3.87 ± 0.04		

All data collected using the UW Micromass IsoProbe. Errors for individual analyses are 2 SE from in run statistics. Average $\delta^{56}Fe$ values are the average of two or more analyses of the same sample solution. The errors for the average $\delta^{56}Fe$ are the external (1 SD) errors; for samples that have been analyzed only once, the error is the 2 SE from the internal statistics. The sample name suffixes, H and S, refer to hematite and solution, respectively.

Table 6. Fe isotope data for long-term exchange between $[Fe^{III}(H_2O)_6]^{3+}$ and hematite (experiment 4).

Sample name	Days incubated	$\delta^{56}Fe$	$\delta^{57}Fe$	Avg. $\delta^{56}Fe$	1 SD or 2 SE
Ex 4-0 H	0	-0.27 ± 0.08	-0.37 ± 0.03	-0.27	0.08
Ex 4-0 S	0	4.83 ± 0.06	7.46 ± 0.06	4.85	0.02
	0	4.86 ± 0.08	7.55 ± 0.07		
Ex 4-1 H	27	0.05 ± 0.07	0.08 ± 0.05	0.05	0.07
Ex 4-2 H	42	-0.12 ± 0.08	-0.08 ± 0.05	-0.12	0.08
Ex 4-2 S	42	4.32 ± 0.07	6.58 ± 0.06	4.35	0.05
	42	4.39 ± 0.06	6.70 ± 0.08		
Ex 4-3 S	58	3.59 ± 0.06	5.45 ± 0.06	3.59	0.06
Ex 4-4 S	83	3.20 ± 0.07	4.85 ± 0.07	3.20	0.07
Ex 4-5 S	98	2.65 ± 0.05	4.02 ± 0.06	2.71	0.08
	98	2.76 ± 0.06	4.16 ± 0.06		

All data collected using the UW Micromass IsoProbe. Errors for individual analyses are 2 SE from in run statistics. Average $\delta^{56}Fe$ values are the average of two or more analyses of the same sample solution. The errors for the average $\delta^{56}Fe$ are the external (1 SD), errors; for samples that have been analyzed only once, the error is the 2 SE from the internal statistics. The sample name suffixes, H and S, refer hematite and solution, respectively.

Table 7. Fe isotope data for long-term exchange between $[Fe^{III}(H_2O)_6]^{3+}$ and hematite (experiment 5).

Sample name	Days incubated	$\delta^{56}Fe$	$\delta^{57}Fe$	Avg. $\delta^{56}Fe$	1 SD or 2 SE
Ex 5-0 H	0	-0.33 ± 0.06	-0.55 ± 0.04	-0.28	0.07
	0	-0.23 ± 0.05	-0.38 ± 0.04		
Ex 5-1 H	28	-0.17 ± 0.11	-0.18 ± 0.08	-0.17	0.11
Ex 5-1 S	28	0.37 ± 0.04	0.66 ± 0.03	0.37	0.04
Ex 5-2 H	54	-0.32 ± 0.12	-0.52 ± 0.09	-0.32	0.12
Ex 5-2 S	54	0.40 ± 0.05	0.64 ± 0.05	0.40	0.05
Ex 5-3 H	67	-0.37 ± 0.10	-0.51 ± 0.07	-0.32	0.05
	67	-0.28 ± 0.06	-0.37 ± 0.03		
	67	-0.31 ± 0.07	-0.45 ± 0.05		
Ex 5-3 S	67	0.29 ± 0.7	0.55 ± 0.05	0.30	0.01
	67	0.30 ± 0.05	0.71 ± 0.04		
Ex 5-4 H	75	-0.28 ± 0.06	-0.37 ± 0.04	-0.28	0.06
Ex 5-4 S	75	0.21 ± 0.08	0.37 ± 0.04	0.20	0.02
	75	0.19 ± 0.04	0.40 ± 0.03		
Ex 5-5 H	128	-0.31 ± 0.05	-0.46 ± 0.03	-0.28	0.05
	128	-0.25 ± 0.05	-0.40 ± 0.03		
Ex 5-5 S	128	-0.07 ± 0.05	0.09 ± 0.02	-0.07	0.05

All data collected using the UW Micromass IsoProbe. Errors for individual analyses are 2 SE from in run statistics. Average $\delta^{56}Fe$ values are the average of two or more analyses of the same sample solution. The errors for the average $\delta^{56}Fe$ are the external (1 SD) errors, for samples that have been analyzed only once, the error is the 2 SE from the internal statistics. The sample name suffixes, H and S, refer to hematite and solution, respectively.

^{57}Fe-enriched runs that dissolution/reprecipitation is the primary means of Fe mass transfer in our experiments. The calculated $\Delta^{56}Fe_{S-H}$ in the model is not defined as kinetic or equilibrium but is merely the value that would be measured and reflects the sum of all of the isotope effects influencing Fe that is being exchanged in the system at a particular time.

Details of the model are given in the Appendix. The model's most important assumptions are that isotopic fractionation occurs only during precipitation, that the $\delta^{56}Fe$ of the bulk and dissolving hematite are the same, and that α^I_{S-H} approaches unity over time along with the precipitation rate; this last assumption only minimally affects the corrections we apply to

$\Delta^{56}Fe^T_{S-H}$ in inferring α^E_{S-H} (see discussion below). That the fractionation factor approaches unity during long-term experiments is well supported by our data, although the exact relationship between the α^I_{S-H} and precipitation rate is not known. The model cannot be used to quantitatively predict $\Delta^{56}Fe_{S-H}$ at particular time intervals but is intended to illustrate the changes in $\Delta^{56}Fe_{S-H}$ that may occur over time and possible relations to α^I_{S-H}, which is the main variable of interest.

Modeled changes in $\Delta^{56}Fe_{S-H}$ as Fe fluxes (dissolution/reprecipitation) decline and α^I_{S-H} approaches unity show a similar pattern regardless of the parameters used (Figs. 8a to 8e). For cases in which experiments begin with $\Delta^{56}Fe_{S-H} = 0$,

Table 8. Fe isotope data for long-term exchange between $[Fe^{III}(H_2O)_6]^{3+}$ and hematite (experiment 6).

Sample name	Days incubated	$\delta^{56}Fe$	$\delta^{57}Fe$	Avg. $\delta^{56}Fe$	1 SD or 2 SE
Ex 6-O H	0	-0.12 ± 0.11	-0.11 ± 0.08	-0.13	0.03
	0	-0.15 ± 0.05	-0.25 ± 0.04		
Ex 6-1 H	35	-0.14 ± 0.05	-0.13 ± 0.04	-0.17	0.05
	35	-0.20 ± 0.05	-0.18 ± 0.03		
Ex 6-1 S	35	0.87 ± 0.06	1.33 ± 0.06	0.83	0.06
	35	0.76 ± 0.05	1.27 ± 0.04		
	35	0.85 ± 0.05	1.41 ± 0.03		
Ex 6-2 H	48	-0.16 ± 0.06	-0.20 ± 0.05	-0.12	0.04
	48	-0.11 ± 0.06	-0.17 ± 0.05		
	48	-0.09 ± 0.06	-0.07 ± 0.04		
Ex 6-2 S	48	0.55 ± 0.08	0.88 ± 0.06	0.51	0.05
	48	0.48 ± 0.07	0.72 ± 0.05		
Ex 6-3 H	56	-0.43 ± 0.12	-0.74 ± 0.06	-0.34	0.14
	56	-0.24 ± 0.06	-0.28 ± 0.05		
Ex 6-4 H	107	-0.23 ± 0.05	-0.28 ± 0.04	-0.24	0.01
	107	-0.25 ± 0.05	-0.36 ± 0.03		
Ex 6-4 S	107	0.65 ± 0.06	1.09 ± 0.03	0.65	0.06

All data collected using the UW Micromass IsoProbe. Errors for individual analyses are 2 SE from in run statistics. Average $\delta^{56}Fe$ values are the average of two or more analyses of the same sample solution. The errors for the average $\delta^{56}Fe$ are the external (1 SD) errors; for samples that have been analyzed only once, the error is the 2 SE from the internal statistics. The sample name suffixes, H and S, refer to hematite and solution, respectively.

Table 9. Fe isotope data for long-term exchange between $[Fe^{III}(H_2O)_6]^{3+}$ and hematite (experiment 7).

Sample name	Days incubated	$\delta^{56}Fe$	$\delta^{57}Fe$	Avg. $\delta^{56}Fe$	1 SD or 2 SE
Ex 7-0 S	0	0.28 ± 0.10	0.47 ± 0.08	0.19	0.13
	0	0.09 ± 0.06	0.19 ± 0.05		
Ex 7-1 S	2	3.55 ± 0.08	5.34 ± 0.04	3.60	0.08
		3.66 ± 0.08	5.33 ± 0.05		
Ex 7-2 H	11	0.40 ± 0.07	0.73 ± 0.06	0.36	0.04
	11	0.33 ± 0.05	0.55 ± 0.03		
	11	0.34 ± 0.04	0.55 ± 0.03		
Ex 7-2 S	11	1.55 ± 0.07	2.36 ± 0.05	1.40	0.20
	11	1.26 ± 0.08	1.99 ± 0.08		
Ex 7-3 H	24	0.40 ± 0.05	0.56 ± 0.05	0.40	0.05
Ex 7-3 S	24	1.41 ± 0.07	2.18 ± 0.04	1.23	0.25
	34	1.05 ± 0.15	1.77 ± 0.05		
Ex 7-4 H	32	0.32 ± 0.05	0.46 ± 0.05	0.34	0.02
	32	0.35 ± 0.07	0.57 ± 0.03		
Ex 7-4 S	32	1.16 ± 0.09	1.84 ± 0.04	1.20	0.06
	32	1.24 ± 0.10	1.87 ± 0.04		
	32	1.04 ± 0.10	1.75 ± 0.05		
Ex 7-5 H	86	0.23 ± 0.05	0.44 ± 0.03	0.23	0.05

All data collected using the UW Micromass IsoProbe. Errors for individual analyses are 2 SE from in run statistics. Average $\delta^{56}Fe$ values are the average of two or more analyses of the same sample solution. The errors for the average $\delta^{56}Fe$ are the external (1 SD) errors; for samples that have been analyzed only once, the error is the 2 SE from the internal statistics. The sample name suffixes, H and S, refer to hematite and solution, respectively.

$\Delta^{56}Fe_{S-H}$ initially rises sharply to its highest value, where the magnitude of the rise depends on the flux. For simulations in which the solution initially contained the steady-state [Fe] (Figs. 8a to 8c), $\Delta^{56}Fe_{S-H}$ rises until it reaches $10^3\ln\alpha^I_{S-H}$, followed closely by an inflection in the $\Delta^{56}Fe_{S-H}$-time curve and then a close tracking of decreasing $\Delta^{56}Fe_{S-H}$ and $10^3\ln\alpha^I_{S-H}$ with time. The model predicts that $\Delta^{56}Fe_{S-H}$ approaches $10^3\ln\alpha^I_{S-H}$ more quickly when Fe fluxes are high than when they are low, and this is also accompanied by a higher

maximum $\Delta^{56}Fe_{S-H}$ value. For relatively low fluxes, $\Delta^{56}Fe_{S-H}$ values approach a constant value that is significantly offset from that of $10^3\ln\alpha^I_{S-H}$ over long time periods (Fig. 8a), as compared with $\Delta^{56}Fe_{S-H}$ values attained during high fluxes (Fig. 8c); this difference is defined as the "terminal offset," that is, $\Delta^{56}Fe^T_{S-H} - 10^3\ln\alpha^I_{S-H}$. The speed with which $\Delta^{56}Fe_{S-H}$ can adjust to changes in $10^3\ln\alpha^I_{S-H}$ is proportional to the Fe flux, and therefore the "terminal offset" for $\Delta^{56}Fe^T_{S-H}$ is in general inversely proportional to precipitation rate. It might at

Table 10. Fe isotope data for long-term exchange between $[Fe^{III}(H_2O)_6]^{3+}$ and hematite (experiment 8).

Sample name	Days incubated	$\delta^{56}Fe$	$\delta^{57}Fe$	Avg. $\delta^{56}Fe$	1 SD or 2 SE
Ex 8-0 H	0	0.30 ± 0.08	0.49 ± 0.05	0.29	0.01
	0	0.28 ± 0.10	0.40 ± 0.06		
Ex 8-0 S	0	0.28 ± 0.10	0.47 ± 0.08	0.19	0.13
	0	0.09 ± 0.06	0.19 ± 0.05		
Ex 8-1 H	13	0.38 ± 0.06	0.73 ± 0.05	0.39	0.02
	13	0.40 ± 0.06	0.69 ± 0.05		
Ex 8-1 S	13	1.10 ± 0.06	1.69 ± 0.04	1.11	0.03
	13	1.13 ± 0.06	1.81 ± 0.05		
Ex 8-2 H	26	0.35 ± 0.07	0.57 ± 0.05	0.38	0.05
	26	0.41 ± 0.06	0.64 ± 0.06		
Ex 8-2 S	26	1.42 ± 0.07	2.26 ± 0.05	1.20	0.21
	26	1.00 ± 0.07	1.62 ± 0.05		
	26	1.17 ± 0.06	1.83 ± 0.03		
Ex 8-3 H	34	0.28 ± 0.05	0.40 ± 0.03	0.28	0.05
Ex 8-3 S	34	1.31 ± 0.06	2.00 ± 0.04	1.29	0.03
	34	1.27 ± 0.11	2.03 ± 0.05		
Ex 8-4 H	84	0.29 ± 0.05	0.56 ± 0.03	0.31	0.03
	84	0.34 ± 0.06	0.61 ± 0.03		
Ex 8-4 S	84	0.95 ± 0.05	1.52 ± 0.03	0.95	0.05

All data collected using the UW Micromass IsoProbe. Errors for individual analyses are 2 SE from in run statistics. Average $\delta^{56}Fe$ values are the average of two or more analyses of the same sample solution. The errors for the average $\delta^{56}Fe$ are the external (1 SD) errors; for samples that have been analyzed only once, the error is the 2 SE from the internal statistics. The sample name suffixes, H and S, refer to hematite and solution, respectively.
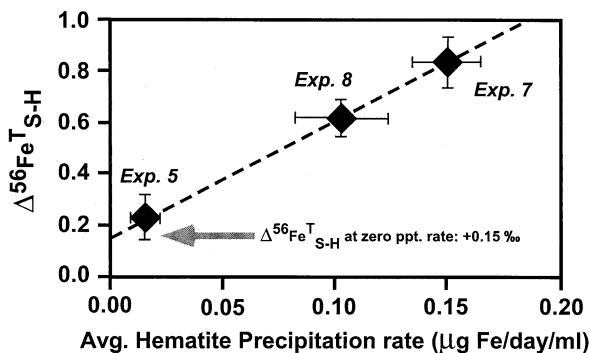
Fig. 7. $\Delta^{56}Fe^{T}_{S-H}$ variations relative to average hematite precipitation rate for experiments that had the lowest hematite precipitation rates and least initial isotope contrast between initial [Fe] and hematite. As noted in the text, $\Delta^{56}Fe^{T}_{S-H}$ is defined as the "terminal $\Delta^{56}Fe_{S-H}$," that is, $\delta^{56}Fe_{S} - \delta^{56}Fe_{H}$ at the end of a particular experiment. Extrapolation to zero precipitation rate is considered to most closely approximate the equilibrium Fe isotope fractionation between solution Fe(III) and hematite, although this value will be offset from the true equilibrium isotope fractionation because of earlier kinetic isotope effects that are not completely erased (see Figs. 8 and 10). Errors in $\Delta^{56}Fe^{T}_{S-H}$ and average hematite precipitation rate shown.

first appear that rapid precipitation rates will provide the closest match between the measured $\Delta^{56}Fe_{S-H}$ and α^{I}_{S-H} (Fig. 8c), but in fact, rapid precipitation rates are more likely to be associated with kinetic isotope fractionation, as shown by the results of experiment 1, and therefore, α^{I}_{S-H} is not expected to approach α^{E}_{S-H} under such conditions.

For experimental conditions in which there is no initial Fe in solution (Fig. 8d), dissolution rates must always exceed precipitation rates at the beginning of incubation. This condition forces [Fe] to rise, eventually causing Fe precipitation to increase as well. When fluxes are low, precipitation rates can adjust to the slowly rising [Fe], and $\Delta^{56}Fe_{S-H}$ is never much greater than $10^{3}\ln\alpha^{I}_{S-H}$. However, if fluxes are higher, initially rapid dissolution may increase [Fe] more rapidly than can be accommodated by precipitation. This effect results in [Fe] overshooting the steady-state value and in a temporary and slightly delayed rise in $\Delta^{56}Fe_{S-H}$ caused by Rayleigh distillation as precipitation forces [Fe] back toward steady state. Under these conditions, $\Delta^{56}Fe_{S-H}$ may significantly exceed $10^{3}\ln\alpha^{I}_{S-H}$ (Fig. 8d). In most simulations, after first rising sharply, [Fe] returns to steady state, and $\Delta^{56}Fe_{S-H}$ then tracks $10^{3}\ln\alpha^{I}_{S-H}$, as described above.

A similar process occurs when Fe is initially present in solution in a concentration above that of the steady-state value, except that in this case, it is precipitation rather than dissolution that dominates the early incubation period. Rapid precipitation drives up $\Delta^{56}Fe_{S-H}$, with the magnitude of the rise depending on the initial [Fe]. After peaking, $\Delta^{56}Fe_{S-H}$ drops and tracks $10^{3}\ln\alpha^{I}_{S-H}$ (Fig. 8e).

The validity of the general trends in $\Delta^{56}Fe_{S-H}$ vs. time for our model may be tested by combining the results of our short-term kinetic experiment (experiment 1), in which α^{I}_{S-H} is far from α^{E}_{S-H}, with those of experiment 7, which had similar initial [Fe] but ran for much longer time periods, resulting in a lower average precipitation rate (Fig. 1, Table 1) The initial increase in $\Delta^{56}Fe_{S-H}$ reflects the kinetic fractionation regime of
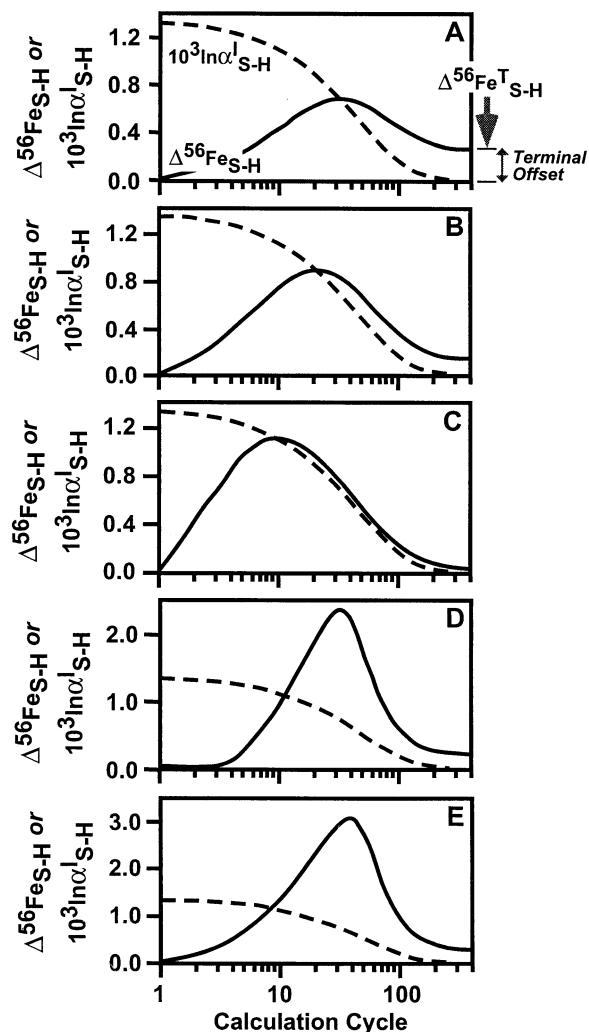

Fig. 8. Modeled changes in $\Delta^{56}Fe_{S-H}$ (solid line) using flux model (see Appendix), as a function of dissolution/precipitation step (calculation cycle) and changes in the instantaneous isotope fractionation, $10^{3}\ln\alpha^{I}_{S-H}$ (dashed line). All models assume that there is no initial isotopic contrast between solution and hematite. (A) Steady-state [Fe] and low-Fe-exchange (precipitation) rates, similar to that calculated for experiment 5 (Table 1). $\Delta^{56}Fe_{S-H}$ rises in response to initially large α^{I}_{S-H} because of initial conditions that include significant kinetic isotope effects. Under steady-state conditions with respect to [Fe], the isotopic "memory" of the initial kinetic effects is not erased even over long time scales and in fact levels out at a constant value. We define the difference between the $\Delta^{56}Fe^{T}_{S-H}$ (marked by arrow) and the instantaneous isotope fractionation factor $10^{3}\ln\alpha^{I}_{S-H}$ as the "terminal offset," which is equal to $\Delta^{56}Fe^{T}_{S-H} - 10^{3}\ln\alpha^{I}_{S-H}$. Through modeling of the terminal offset as a function of precipitation rate, we can estimate the equilibrium isotope fractionation factor α^{E}_{S-H}, assuming $\alpha^{I}_{S-H} \to \alpha^{E}_{S-H}$ at long time scales. (B) Steady-state conditions similar to those used in (A), except at higher precipitation rates; the modeled precipitation rate is similar to the rate in experiment 7 (Table 1). (C) Steady-state conditions similar to those used in (B), except at very high precipitation rates, between those of experiments 6 and 7 (Table 1). Note that the terminal offset decreases with increasing precipitation rates (parts A, B, and C). (D) Simulation in which no initial Fe is present, such as in experiments 5 and 6, at moderate Fe precipitation rates (similar to that of experiment 8). (E) Simulation in which initial solution [Fe] is very high and Fe precipitation rates are moderate, equal to those of experiment 7.
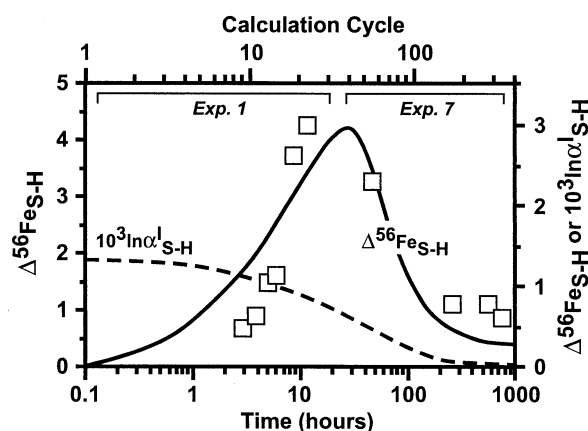
Fig. 9. Superposition of modeled $\Delta^{56}Fe_{S-H}$ (solid line) and $10^3\ln\alpha^I_{S-H}$ (dashed line) variations at high initial solution [Fe] and moderate precipitation rates (conditions of experiment 7; Fig. 8e), with the most pertinent experimental data (open squares). Over short time scales (≤ 12 h), kinetic isotope fractionation produced in experiment 1 is applicable, whereas over longer time scales, data from experiment 7 are applicable. Scales for measured data on left and bottom, whereas scales for model (from Fig. 8e), on right and top. As discussed in text, direct applicability of modeled variations to entire time scale of experiments (from hours to scores of days) is limited because calculation cycles cannot be linearly scaled to time; it is generally expected that the time interval of a calculation cycle increases with absolute time because ^{57}Fe tracer experiments show that the flux of Fe during dissolution/reprecipitation drops to zero over time (Fig. 6).

experiment 1, similar to a model in which high [Fe] and moderate to high Fe fluxes occur (Fig. 8e), followed by a decrease in $\Delta^{56}Fe_{S-H}$ as α^I_{S-H} approaches unity, and more closely approximates α^E_{S-H} (Fig. 9). It is important to note the goal of our modeling is not to precisely match our experimental data; the primary difficulty in relating our model to measured data lies in the fact that one dissolution/precipitation cycle in the model is not expected to linearly track time over the course of the experiment. Despite this scaling difficulty, however, the modeled trends generally match those measured in the experiments (Fig. 9).

4. DISCUSSION

The model we have developed to explain the isotopic variations as a function of Fe fluxes can be used to correct for the "memory" effects of the initial kinetic-dominated phase of our experiments. This results in a calculated equilibrium Fe isotope fractionation factor that is significantly different from that predicted from spectroscopic data.

4.1. Calculation of the Equilibrium Fractionation Factor

The ultimate goal of the current study is to determine the equilibrium Fe isotope fractionation factor between $[Fe^{III}(H_2O)_6]^{3+}$ and hematite (α^E_{S-H}). Because it is impossible to obtain complete true isotope exchange reactions at the low temperatures of our experiments, even on time scales approaching 1 yr, we ultimately infer α^E_{S-H} on the basis of extrapolation to very low precipitation rates; this approach has been commonly used for O isotopes, for example, in carbonate and oxide

systems (e.g., Carothers et al., 1988; Yapp, 1990; Kim and O'Neil, 1997). As noted above, the terminal offset between $\Delta^{56}Fe^T_{S-H}$ and α^I_{S-H} is largest when fluxes are lowest. At the same time, however, we assume that it is in experiments that have the lowest fluxes (precipitation rates) that α^I_{S-H} most closely approaches the equilibrium fractionation factor α^E_{S-H}. Therefore, we interpret $\Delta^{56}Fe^T_{S-H}$ as an upper limit to both α^I_{S-H} at the end of each experiment and on α^E_{S-H}. Experiment 5 had the lowest precipitation rate (Fig. 1) and also the smallest $\Delta^{56}Fe^T_{S-H}$ (Fig. 7), and this experiment is considered to most likely approach α^E_{S-H}.

Our model predicts that during periods when $\Delta^{56}Fe_{S-H}$ is steadily declining, the offset between $\Delta^{56}Fe_{S-H}$ and $10^3\ln\alpha_{S-H}$ is approximately constant for a given flux (Fig. 8). This relation makes it possible to calculate the terminal offset ($\Delta^{56}Fe^T_{S-H} - 10^3\ln\alpha^E_{S-H}$) for different Fe precipitation rates (Fig. 10a) and to correct the observed $\Delta^{56}Fe^T_{S-H}$ to $10^3\ln\alpha^E_{S-H}$ (Fig. 10b), assuming that the system has reached the condition $\alpha^I_{S-H} = \alpha^E_{S-H}$. The corrected values are, of course, model dependent, and this compounds any error in the measured isotopic compositions. A regression through observed $\Delta^{56}Fe^T_{S-H}$ values relative to Fe precipitation rates, extrapolated to zero precipitation rate, produces a $\Delta^{56}Fe^T_{S-H}$ of $+0.15‰$ (Fig. 7). In contrast, application of the terminal offset ($\Delta^{56}Fe^T_{S-H} - 10^3\ln\alpha^E_{S-H}$) relation in Fig. 10a to the data in Fig. 7 produces a revised regression, extrapolated to zero precipitation rate, for which $\Delta^{56}Fe^T_{S-H} = -0.14‰$ (Fig. 10b). If model parameters such as exchange rate and [Fe] are varied as to encompass those of our experiments, the curve in Fig. 10a is only slightly affected; the intercept of the corrected regression (Fig. 10b) would vary between -0.20 and $0.00‰$ over this range. Using this uncertainty, as well as those of the measured data, we therefore estimate that $10^3\ln\alpha^E_{S-H} = -0.10 \pm 0.20‰$ for the $^{56}Fe/^{54}Fe$ isotope fractionation between $[Fe^{III}(H_2O)_6]^{3+}$ and hematite at 98°C.

4.2. Comparison With Theoretical Predictions

There have been several recent studies that calculated equilibrium Fe isotope fractionations among minerals and fluids, and our results provide important tests of these predictions. Reduced partition function ratios ($\beta_{56/54}$) for Fe-bearing minerals have been calculated on the basis of modeling ^{57}Fe Mössbauer data (Polyakov, 1997; Polyakov and Mineev, 2000), whereas $\beta_{56/54}$ factors for a number of aqueous Fe species have been calculated using a modified Urey-Bradley force field model applied to vibrational frequencies obtained from spectroscopic and neutron-scattering data (Schauble et al., 2001). Iron isotope fractionations between common oxide minerals and aqueous Fe complexes may be derived by combining the two sets of $\beta_{56/54}$ factors through the following relation:

$$10^3\ln\alpha_{A-B} = 10^3\ln\beta_A - 10^3\ln\beta_B.$$

Very large equilibrium fractionations in $^{56}Fe/^{54}Fe$ are predicted at low temperature between $[Fe^{III}(H_2O)_6]^{3+}$ and goethite, hematite, and magnetite (Fig. 11), as high as 5 to 6‰, when the Mössbauer- and vibrational frequency–derived $\beta_{56/54}$ factors are combined. Our estimate for the equilibrium $10^3\ln\alpha_{Fe(III)-hematite}$ at 98°C of $-0.10 \pm 0.20‰$ is significantly
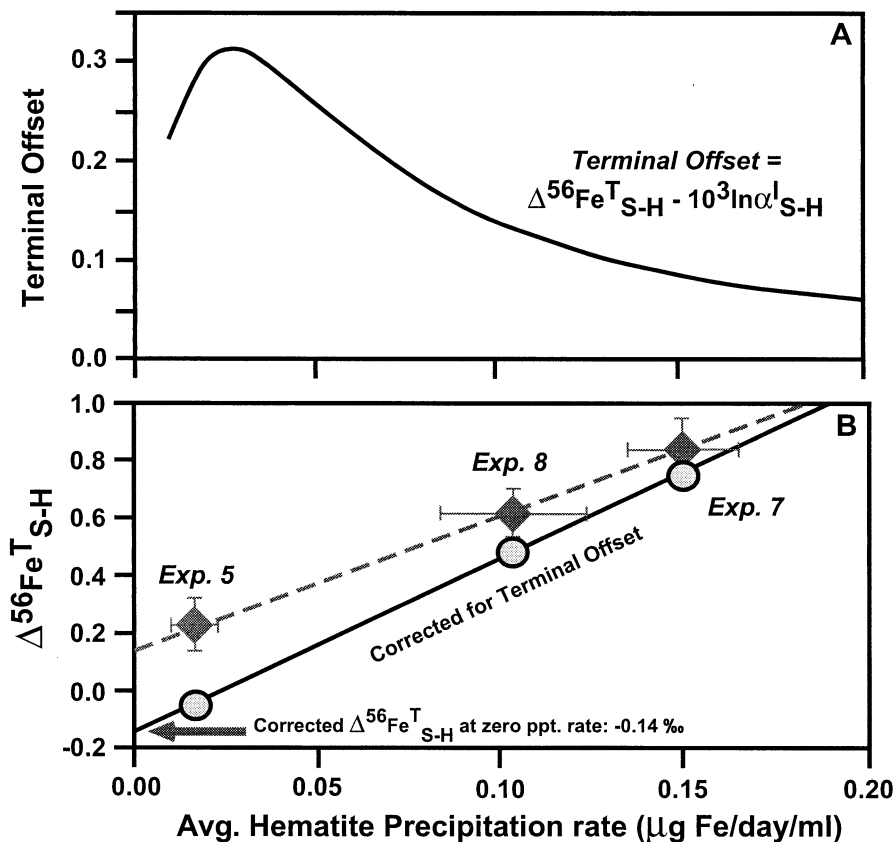
Fig. 10. Correction of $\Delta^{56}Fe^T_{S-H}$ values for terminal offset (see Fig. 8a), as a function of average hematite precipitation rate. (A) As shown in Figs. 8a to 8c, the terminal offset generally decreases with the increasing Fe precipitation rate, and this can be used to correct the measured $\Delta^{56}Fe^T_{S-H}$ values for the long-term experiments to obtain a closer estimation of the equilibrium Fe isotope fractionation factor α^E_{S-H}, assuming $\alpha^I_{S-H} \rightarrow \alpha^E_{S-H}$ at long time scales. (B) Measured (from Fig. 7) and corrected $\Delta^{56}Fe^T_{S-H}$ values relative to average hematite precipitation rate for experiments 5, 7, and 8. Corrected $\Delta^{56}Fe^T_{S-H}$ values based on curve in (A); extrapolation of trend of corrected $\Delta^{56}Fe^T_{S-H}$ values to zero precipitation rates yields a $\Delta^{56}Fe^T_{S-H}$ value of -0.14‰. Variation of model parameters for the curve in (A) over the range of our experiments produces an estimate of the corrected $\Delta^{56}Fe^T_{S-H}$ at zero precipitation rate of -0.10 ± 0.20‰. Assuming that at long time scales and slow (near zero) precipitation rates $\alpha^I_{S-H} \rightarrow \alpha^E_{S-H}$, this estimate can be set equivalent to $10^3 ln\alpha_{S-H} = -0.10 \pm 0.20$‰ for the equilibrium Fe isotope fractionation between Fe(III) and hematite at 98°C.

smaller than that predicted using the $\beta_{56/54}$ factors from Polyakov (1997), Polyakov and Mineev (2000), and Schauble et al. (2001) (Fig. 11). In addition to the experimental constraints provided here, additional support for relatively small equilibrium Fe(III)-oxide fractionations comes from the range of $\delta^{56}Fe$ values observed in natural oxides, which generally do not exceed ~2‰ (Beard et al., in press). We also infer that the equilibrium Fe(III)-hematite fractionation lies close to zero at temperatures lower than those of our study, given the unlikely possibility that the slopes of the equilibrium Fe(III)-hematite fractionation on a $10^3 ln\alpha_{Fe(III)-hematite}$-$10^6/T^2$ plot are as steep as those predicted by the Mössbauer- and vibrational frequency–derived $\beta_{56/54}$ factors (Fig. 11); although it is possible that Fe isotope fractionation between Fe(III) and hematite exhibits a crossover, as may be seen for oxygen isotopes for some oxides (e.g., O'Neil and Clayton, 1964), we see no justification in invoking such a phenomenon in the absence of experimental data.

Additional constraints on evaluating predicted Fe isotope fractionations come from the experimental determination of the

equilibrium isotope fractionation between $[Fe^{III}(H_2O)_6]^{3+}$ and $[Fe^{II}(H_2O)_6]^{2+}$, which has been determined by Johnson et al. (2002) at 22°C and is plotted in Fig. 11. Although the predicted Fe(III)-Fe(II) fractionation is similar in sign to that measured, the magnitude of the predicted fractionation is too large by ~2.5‰ (Fig. 11), consistent with the excessively large predicted Fe(III)-hematite fractionation as compared to that obtained in our experiments. These observations may be tentatively taken to indicate that the $\beta_{56/54}$ factors for $[Fe^{III}(H_2O)_6]^{3+}$ reported by Schauble et al. (2001) are too large by several per mil in the temperature range of 0 to 100°C, although consideration of $\delta^{56}Fe$ values of natural magnetite, hematite, and siderite also suggests that the differences in $\beta_{56/54}$ factors for these minerals calculated by Polyakov and Mineev (2000) are also too large (Beard et al., in press).

5. CONCLUSIONS

A detailed investigation of Fe isotope fractionation between $[Fe^{III}(H_2O)_6]^{3+}$ and hematite at 98°C allows the equilibrium
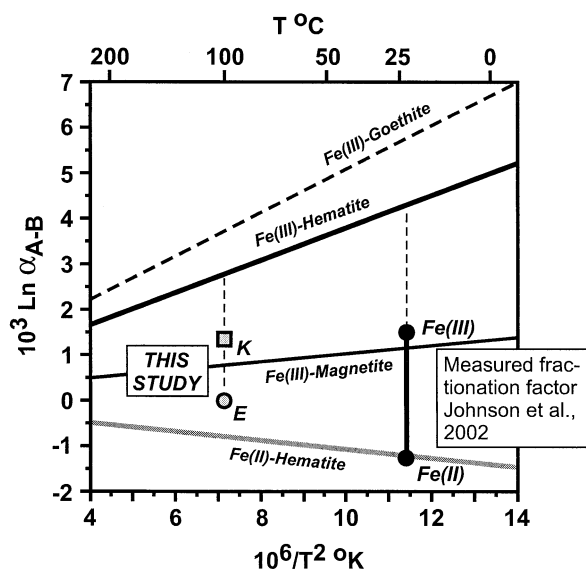
Fig. 11. Comparison of predicted Fe isotope fractionation between solution Fe and iron oxides with experimentally determined equilibrium isotope fractionation factors. The labeled curves are predicted isotope fractionations based on reduced partition function ratios (calculated as $\beta_{56/54}$) from Polyakov (1997), Polyakov and Mineev (2000) and Schauble et al. (2001). The predicted isotopic fractionations between $[Fe^{III}(H_2O)_6]^{3+}$ and hematite at 98°C are much larger than the approximately zero equilibrium fractionation (E) determined in this study, as well as the kinetic (K) fractionation reported here. For comparison, the equilibrium isotope fractionation between $[Fe^{III}(H_2O)_6]^{3+}$ and $[Fe^{III}(H_2O)_6]^{2+}$ at 22°C determined by Johnson et al. (2002) is also shown, relative to the predicted Fe(III)-hematite and Fe(II)-hematite fractionation (lower limit fixed on Fe[II]-hematite curve to aid in comparison).

$56Fe/54Fe$ fractionation to be inferred, which produces $10^3\ln\alpha_{Fe(III)-hematite} = -0.10 \pm 0.20‰$. Because true isotope exchange reactions cannot be obtained at the low temperatures of the current study, the equilibrium Fe isotope fractionation is inferred from long-term (up to 203 d) incubation experiments in which hematite undergoes very slow dissolution/reprecipitation rates. The equilibrium Fe(III)-hematite fractionation factor determined in this study is significantly smaller than that obtained from the reduced partition function ratios calculated for $[Fe^{III}(H_2O)_6]^{3+}$ and hematite on the basis of Mössbauer shifts and vibrational frequencies by Polyakov (1997) and Polyakov and Mineev (2000) and Schauble et al. (2001), respectively, which is +2.9‰ for $10^3\ln\alpha_{Fe(III)-hematite}$ at 100°C. Assuming that the slope of Fe(III)-hematite fractionation is modest relative to $10^6/T^2$, we infer that this fractionation remains close to zero at lower temperatures. These results suggest that $\delta^{56}Fe$ values of hematite may accurately reflect the Fe isotope composition of ferric iron in solution, providing a critical link for inferring the Fe isotope compositions of ancient fluids from the rock record.

The inferred equilibrium isotope fractionation between $[Fe^{III}(H_2O)_6]^{3+}$ and hematite is significantly smaller than that of kinetic fractionations obtained in the same experimental design but that involved rapid hematite precipitation rates; these results produced isotopically zoned hematite crystals that may be described by a Rayleigh distillation process where

$10^3\ln\alpha_{S-H} = +1.3‰$. In contrast, simple dissolution, under conditions in which simultaneous precipitation does not occur, does not produce significant isotopic fractionation, <0.1‰, as expected on the basis of dissolution mechanisms and consideration of rates of solid-state diffusion. Distinction between kinetic and equilibrium isotope fractionations in laboratory experiments is essential, and assessment of the extent of isotopic zonation produced by possible kinetic processes may be done by stepwise leaching in concentrated acids. Such an approach holds promise for detecting nonequilibrium Fe isotope fractionations in natural mineral samples.

REFERENCES

Anbar A. D., Roe J. E., Barling J., and Nealson K. H. (2000) Nonbiological fractionation of iron isotopes. *Science* **288**, 126–128.

Bao H. and Koch P. L (1999) Oxygen isotope fractionation in ferric oxide-water systems: Low temperature synthesis. *Geochim. Cosmochim. Acta* **63**, 599–613.

Bao H., Koch P. L., and Thiemens M. H. (2000) Oxygen isotopic composition of ferric oxides from recent soil, hydrologic, and marine environments. *Geochim. Cosmochim. Acta* **64**, 2221–2231.

Beard B. L. and Johnson C. M. (1999) High-precision iron isotope measurements of terrestrial and lunar materials. *Geochim. Cosmochim. Acta* **63**, 1653–1660.

Beard B. L., Johnson C. M., Cox L., Sun H., Nealson K. H, and Aguilar C. (1999) Iron isotope biosignatures. *Science* **285**, 1889–1892.

Beard B. L., Johnson C. M., Skulan J. L., Nealson K. H., Cox L., and Sun H. (in press) Application of Fe isotopes to tracing the geochemical and biological cycling of Fe. *Chem. Geol.*

Brantley S. L., Liermann L., and Bullen T. D. (2001) Fractionation of Fe isotopes by soil microbes and organic acids. *Geology* **29**, 535–538.

Bullen T. D., White A. F., Childs C. W., Vivit D. V., and Schultz M. S. (2001) Demonstration of significant abiotic iron isotope fractionation in nature. *Geology* **29**, 699–702.

Carothers W. W., Adami L. H., and Rosenbauer R. J. (1988) Experimental oxygen isotope fractionation between siderite-water and phosphoric-acid liberated CO_2-siderite. *Geochim. Cosmochim. Acta* **52**, 2445–2450.

Clayton R. N. and Epstein S. (1961) The use of oxygen isotopes in high-temperature geological thermometry. *J. Geol.* **69**, 447–452.

Cornell R. M. and Giovanoli R. (1993) Acid dissolution of hematites of different morphologies. *Clay Miner.* **28**, 223–232.

Dawson M. and Lyle S. (1990) Spectrophotometric determination of iron and cobalt with Ferrozine and dithiozone. *Talanta* **37**, 1189–1192.

Dubinina E. O. and Laakshtanov L. Z. (1997) A kinetic model of isotope exchange in dissolution-precipitation processes. *Geochim. Cosmochim. Acta* **61**, 2265–2273.

Hair N. J. and Beattie J. K. (1977) Structure of hexaaqua iron (III) nitrate trihydrate. Comparison of iron (II) and iron (III) bond lengths in high-spin octahedral environments. *Inorg. Chem.* **16**, 245–250.

Johnson C. M. and Beard B. L. (1999) Correction of instrumentally produced mass fractionation during isotopic analysis of Fe by thermal ionization mass spectrometry. *Int. J. Mass Spectrom.* **193**, 87–99.

Johnson C. M., Skulan J. L., Beard B. L Sun H., Nealson K. H., and Braterman P. S. (2002) Isotopic fractionation between Fe(III) and Fe(II) in aqueous solutions. *Earth Planet. Sci. Lett.* **195**, 141–153.

Kanno H. and Hiraishi J. (1982) A Raman study of aqueous solutions of ferric nitrate, ferrous chloride and ferric chloride in the glassy state. *J. Raman Spectrosc.* **12,** 224–227.

Kieffer S. W. (1982) Thermodynamics and lattice vibrations of minerals: 5. Applications to phase equilibria, isotopic fractionation, and pressure thermodynamic properties. *Rev. Geophys. Space Phys.* **20,** 827–849.

Kim S.-T. and O'Neil J. R. (1997) Equilibrium and nonequilibrium oxygen isotope effects in synthetic carbonates. *Geochim. Cosmochim. Acta* **61,** 3461–3475.

Magini M. (1978) An X-ray investigation on the structure of iron(III) perchlorate solutions. *J. Inorg. Nucl. Chem.* **40,** 43–48.

Magini M. and Caminiti R. (1977) On the structure of highly concentrated iron(III) salt solutions. *J. Inorg. Nucl. Chem.* **39,** 91–94.

Matijevic E. and Scheiner P. (1978) Ferric hydrous oxide sols, III, preparation of uniform particles by hydrolysis of Fe(III)-chloride, -nitrate, and -percholorate solutions. *J. Colloid Interface Sci.* **63,** 509–524.

Matsuhisa Y., Goldsmith J. R., and Clayton R. N. (1978) Mechanism of hydrothermal recrystallization of quartz at 250°C and 15 kb. *Geochim. Cosmochim. Acta* **42,** 173–183.

Maurice P. A., Hochella M. F., Parks G. A., Sposito G., and Schwertmann U. (1995) Evolution of hematite surface microtopography upon dissolution by simple organic acids. *Clays Clay Miner.* **43,** 29–38.

O'Neil J. R. (1986) Theoretical and experimental aspects of isotopic fractionation. In *Stable Isotopes in High Temperature Geological Processes,* Vol. 16 (eds. J. W. Valley, et al), pp. 1–40. Mineralogical Society of America, Washington, DC Rev. Mineral..

O'Neil J. R. and Clayton R. N. (1964) Oxygen isotope geothermometry. In *Isotopic and Cosmic Chemistry* (eds. H. Craig, S. L. Miller, and G. J. Wasserburg), pp. 157–168. North Holland-Amsterdam, the Netherlands.

Ozden O. and Dunlop D. J. (2000) Intermediate magnetite formation during dehydration of goethite. *Earth Planet. Sci. Lett.* **117,** 59–67.

Polyakov V. B. (1997) Equilibrium fractionation of the iron isotopes: Estimation from Mössbauer spectroscopy data. *Geochim. Cosmochim. Acta* **61,** 4213–4217.

Polyakov V. B. and Mineev S. D. (2000) The use of Mössbauer spectroscopy in stable isotope geochemistry. *Geochim. Cosmochim. Acta* **64,** 849–865.

Samson S. D., Stillings L. L., and Eggleston C. M. (2000) The depletions and regeneration of dissolution-active sites at the mineral-water interface: I. Fe, Al, and In sesquioxides. *Geochim. Cosmochim. Acta* **64,** 3471–3484.

Schauble E. A., Rossman G. R., and Taylor H. P. (2001) Theoretical estimates of equilibrium Fe-isotope fractionations from vibrational spectroscopy. *Geochim. Cosmochim. Acta* **65,** 2487–2497.

Schwertmann U. and Cornell R. M. (1991) *Iron Oxides in the Laboratory: Preparation and Characterization.* VCH Publishers, Weinheim, Germany.

Skulan J. L., Sun H., Beard B., O'Leary J., Johnson C., Nealson K. (2000) Progress in the development of an iron isotope biosignature. *Eos: Trans. Am. Geophys. Union,* May 9, 2000, supplement S30.

Taylor P. D. P., Maeck R., and De Bièvre P. (1992) Determination of the absolute isotopic composition and atomic weight of a reference sample of natural iron. *Int. J. Mass Spectrom. Ion Processes* **121,** 111–125.

Taylor P. D. P., Maeck R., Hendrickx F., and De Bièvre P. (1993) The gravimetric preparation of synthetic mixtures of iron isotopes. *Int. J. Mass Spectrom. Ion Processes* **128,** 91–97.

van der Walt T. N. and Strelow F. (1985) Separation of iron-52 from chromium cyclotron targets on the 2% cross-linked anion-exchange resin AG1-X2 in hydrochloric acid. *Talanta* **32,** 313–317.

Yapp C. J. (1987) Oxygen and hydrogen isotope among goethites (□-FeOOH) and the determination of paleotemperatures. *Geochim. Cosmochim. Acta* **51,** 355–364.

Yapp C. J. (1990) Oxygen isotopes in iron(III) oxides: 1, Mineral-water fractionation factors. *Chem. Geol.* **85,** 329–335.

Zhu X. K., O'Nions R. K., Guo Y. L., and Reynolds B. C. (2000) Secular variation of iron isotopes in North Atlantic deep water. *Science* **287,** 2000–2002.
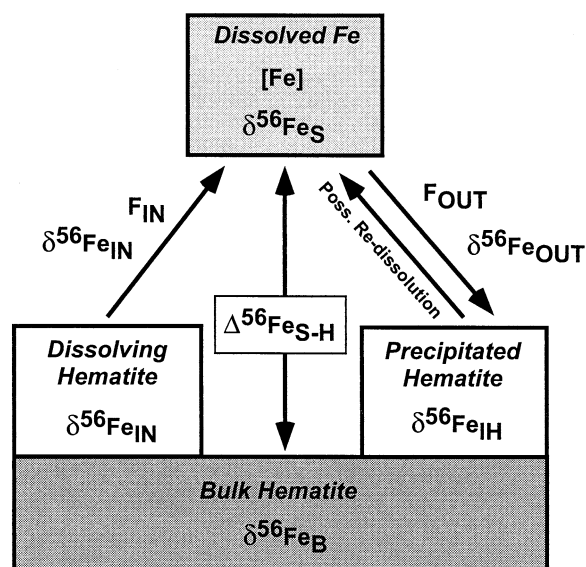
Fig. A1. Box model for flux model discussed in Appendix and presented in Figs. 8 to 10. See Appendix for detailed discussion.

APPENDIX

As described in the main body of the paper, the model used here reproduces the general behavior of the experiments but cannot predict the exact behavior of $\Delta^{56}Fe_{S-H}$ for any particular experiment. The model (Fig. A1) makes several assumptions:

1. Fe isotope exchange occurs via a dissolution-precipitation process.
2. Fe isotope fractionation occurs only during precipitation.
3. The isotopic composition of Fe that is dissolved from hematite does not change.
4. The Fe precipitation rate is positively correlated with [Fe], whereas the Fe dissolution rate is negatively correlated with [Fe].
5. The rate of hematite dissolution slows over time as the result of depletion of active dissolution sites (eg., Cornell and Giovanoli, 1993). If this is true, precipitation rate must also decrease.
6. The instantaneous solution-hematite isotope fractionation factor (α^I_{S-H}) drops over time, probably (but not necessarily) as the result of decreasing precipitation rate.
7. The precipitation rate is tied to the dissolution rate because both affect, and are affected by, [Fe] However, because the hydrolysis reaction takes time to initiate, the precipitation rate does not instantaneously react to changes in dissolution rate. We take an iterative approach to modeling the overall exchange reaction because time delays are easily incorporated in such a model.

As written, the model reaches steady state when [Fe] = 1.0 (arbitrary units). Measured steady-state values of [Fe], and also measured exchange rates, must be corrected to this value before they are used as inputs into the model.

Once initial conditions are set, the model solves for the following variables:

1. [Fe] Under most conditions, values of [Fe] below 1.0 result in an initial rise in $\Delta^{56}Fe_{S-H}$ of the solution. The magnitude of this rise is highly dependent on the actual value of [Fe] that is selected and becomes implausibly large when [Fe] is lower than ~0.05. Therefore, when modeling experiments in which the initial [Fe] is zero, initial [Fe] in the model must be set at a finite though very small number greater than zero No attempt has been made to correct this boundary issue, in part because rapid increase in $\Delta^{56}Fe_{S-H}$ is a real phenomenon, easily explained by the inability of precipitation rates to instantaneously adjust to changes in [Fe], and partly because detailed knowledge of the dissolution kinetics of hematite under the experimental conditions would be required.

2. $\delta^{56}Fe_S$, the $\delta^{56}Fe$ of the solution.
3. $\delta^{56}Fe_{IH}$, the instantaneous $\delta^{56}Fe$ of hematite (ie., the $\delta^{56}Fe$ of hematite actually precipitated during a particular step).
4. α^{I}_{S-H}, the instantaneous isotope fractionation factor In the model, α^{I}_{S-H} is arbitrarily forced to decline exponentially each step by K^{n}_{A}, where K_A is a number >0 and <1 (in practice, usually 0.98 or higher), and n is the iteration step in the calculation.
5. $\delta^{56}Fe_{SS}$, the steady-state $\delta^{56}Fe$ of solution, assumed to be equal to $10^3 \ln\alpha^{I}_{S-H} + \delta^{56}Fe_{IH}$.
6. F_{IN}, the flux of Fe into solution (dissolution flux) In the model, F_{IN} is forced to decline each step by K^{n}_{EX}, where K_{EX} is a number >0 and <1 (in practice, usually 0.98 or higher), and n is the iteration step in the calculation.
7. F_{OUT}, the flux of Fe out of solution (precipitation flux) F_{OUT} is forced to decline along with F_{IN}.
8. $\delta^{56}Fe_B$, the $\delta^{56}Fe$ of the bulk hematite; the measured Fe isotope composition of hematite.

The model iteratively solves for these variables using the following equations:

$$[Fe]_n = [Fe]_{n-1} + Fe_{IN\,n-1} - Fe_{OUT\,n-1}.$$

$$\delta^{56}Fe_{S,n} = [([Fe]_{n-1} \times \delta^{56}Fe_{S,n}) + (Fe_{IN\,n-1} \times H)$$
$$- (Fe_{OUT\,n-1} \times \delta^{56}Fe_{IH\,n-1})]/([Fe]_{n-1} + Fe_{IN\,n-1} - Fe_{OUT\,n-1}).$$

$$\delta^{56}Fe_{IH,n} = \delta^{56}Fe_{S,n} - [(\alpha^{I}_{S-H,n} - 1) \times 1000].$$

$$\alpha^{I}_{S-H,n} = 1 + (0.0013 \times K^{n}_{A});$$

this sets the initial $\Delta^{56}Fe_{S-H}$ equal to 1.3‰, the value measured in the kinetic fractionation experiment (experiment 1).

$$\Delta^{56}Fe_{SS,n} = \delta^{56}Fe_{S,n} - \delta^{56}Fe_{IH,n}.$$

$$Fe_{IN,n} = EX \times (1/[Fe]_{n-1}) \times K^{n}_{EX}.$$

$$Fe_{OUT,n} = EX \times [Fe]_{n-1} \times K^{n}_{EX},$$

where n is the iteration number in the calculation, H is the (constant) isotope composition of the bulk hematite, and EX is the Fe exchange rate. The units of EX are arbitrary, but approximately μg Fe/d/mL, corrected to a steady concentration of 1 ppm. The model is designed to work with EX values below $\sim$0.3. At higher EX values, the model predicts oscillations in [Fe] and isotope compositions. As EX increases, these oscillations become unrealistically large and eventually drive [Fe] below zero, which of course is impossible.